

c) Enzyme Linked Aptamer Assay (ELAA) analysis

To validate the results obtained from SPR and EMSA analysis, direct-ELAA was conducted by first immobilizing 50 μL /well of 20 $\mu\text{g}/\text{mL}$ RBP4 protein in 50 mM carbonate-bicarbonate buffer (pH 9.0) in a polystyrene 96-well microtiter plate. The plate was then incubated for 30 min at 25 $^{\circ}\text{C}$. The buffer containing the unbound RBP4 protein was decanted and the plate was washed three times with 200 μL of washing buffer (1 \times PBS containing 0.05% Tween 20 pH 7.4). The wells were blocked with 200 μL of 5% skim milk powder in PBS-tween 20 pH 7.4 for 30 min at 25 $^{\circ}\text{C}$, followed by three more washes with 200 μL of washing buffer. A total of 50 μL of 100 nM biotinylated RBA-1 in 1 \times SELEX buffer was added to each well and the plate was incubated at 25 $^{\circ}\text{C}$ for 30 min. The buffer containing the unbound aptamer was decanted and the wells were washed three times with 200 μL of washing buffer. To each well 50 μL of 0.5:10000 dilutions of SA-poly HRP (1 mg/mL stock) was added, followed by an incubation at 25 $^{\circ}\text{C}$ for 30 min. The wells were then washed five times with 200 μL of washing buffer. Thereafter, 50 μL of TMB substrate solution was added to each well and incubated for 15 min at 25 $^{\circ}\text{C}$, in the dark. The reaction was stopped by the addition of 50 μL /well of 0.5 M H_2SO_4 and the optical density was measured at 450 nm using the SpectraMax 340PC384. The above experiment was followed for the biotinylated RBA-2/15 mer' poly-T.

2.2.2.3 Identification of dual aptamers for RBP4

a) Characterization of dual aptamers for RBP4 by SPR

The duality of these aptamers were evaluated using a sandwich based SPR. The same equipment as described in **Section 2.2.1.3** was used. After insertion of the Au sensor chips, the sensor chips were primed using KH_2PO_4 (1 M, pH 3.8). This was followed by activating channel one on the sensor chip, using EDC/NHS buffer (35 μL of a 4:1 mixture of EDC (400 mM) and NHS (100 mM), at a flow rate of 5 $\mu\text{L}/\text{min}$. The thiolated RBA-2 aptamer, at a final concentration of 10 μM , was prepared in KH_2PO_4 (1 M, pH 3.8) and 50 μL was injected into channel two, at a flow rate of 5 $\mu\text{L}/\text{min}$. Following immobilization of the thiolated RBA-2, any excessive groups were deactivated by injecting 20 μL 10 mM of 6-mercapto-1-hexanol. To remove the unbound proteins, the sensor chip surface was then regenerated three times, by injecting 35 μL of NaCl/NaOH buffer (2 M/50 mM) at a flow rate of 5 $\mu\text{L}/\text{min}$. RBP4 protein was diluted in 1 \times SELEX buffer to a final concentration of 100 nM and injected for 6 min at

a flow rate of 10 $\mu\text{L}/\text{min}$. The baseline was allowed to stabilise by allowing the selection buffer to flow over the sensor chip for approximately 1-2 hrs. Subsequently, 50 μL of each aptamer (RBA-2, RBA-3 and RBA-3) at increasing concentrations (31.25 - 1000 nM), prepared in 1 \times SELEX buffer, were injected for 6 min at a flow rate of 5 $\mu\text{L}/\text{min}$. Thereafter, 200 $\mu\text{g}/\text{mL}$ of streptavidin was injected for 6 min at a flow rate of 5 $\mu\text{L}/\text{min}$. The sensor chip was then regenerated, three times, as previously described; and the baseline was allowed to stabilise by allowing the selection buffer to flow over the sensor chip for approximately 1-2 hrs. SPR data analysis was performed using BIAevaluation software.

b) Characterization of dual aptamers for RBP4 by ELAA

To validate the results obtained from the sandwich-SPR analysis, an ELAA was conducted by washing the melaimide activated plate with 200 $\mu\text{L}/\text{well}$ of washing buffer (1 \times PBS containing 0.05% Tween 20 pH 7.4). The wells were coated with 50 μL of 20 nM of thiolated aptamer in 1 \times PBS buffer and incubated at 25 $^{\circ}\text{C}$, overnight. The buffer containing the unbound RBP4 was decanted and the plate was washed three times with 200 μL of washing buffer (1 \times PBS containing 0.05% Tween 20 pH 7.4). The wells were blocked with 200 μL of 5% skim milk powder in PBS-tween 20 (pH 7.4) for 30 min at 25 $^{\circ}\text{C}$, followed by three more washes with 200 μL of washing buffer. A total of 50 μL of 100 $\mu\text{g}/\text{mL}$ RBP4, made in 1 \times SELEX buffer, was added to each well and incubated at 25 $^{\circ}\text{C}$ for 30 min, followed by washing the wells three times with 200 μL of washing buffer. Then, 50 μL of different concentration (1 - 100 nM) of the 5'-biotinylated RBA (RBA-1, RBA-2 and RBA-3) in 1 \times SELEX buffer were added to the wells, and followed by incubation at 25 $^{\circ}\text{C}$ for 30 min. The buffer containing the unbound aptamer was decanted and the wells were washed three times with 200 μL of washing buffer. To each well, 50 μL of 0.5:10000 dilutions of SA-poly HRP (1 mg/mL stock) was added, followed by an incubation at 25 $^{\circ}\text{C}$ for 30 min. The wells were then washed five times with 200 μL of washing buffer. Thereafter, 50 μL of TMB substrate solution was added to each well and incubated for 15 min at 25 $^{\circ}\text{C}$ in the dark. The reaction was stopped by the addition of 50 $\mu\text{L}/\text{well}$ of 0.5 M H_2SO_4 and the optical density was measured at 450 nm using the SpectraMax 340PC384.

2.2.3 Synthesis and characterization of AuNPs

AuNPs were prepared by citrate reduction of HAuCl_4 according to the previously reported protocol (Sibuyi *et al.*, 2017). After the synthesis, characterizations were done with respect to the optical properties using the following techniques:

2.2.3.1 UV-vis spectrophotometric analysis

To measure the absorbance spectra, 100 μL of the AuNP sample was added in a flat bottom Greiner 96 well plate and the absorbance's were measured using a POLARstar Omega microplate reader set to a wavelength (λ) range of 400 to 700 nm. The data was analyzed using Microsoft Excel.

2.2.3.2 Hydrodynamic size, Polydispersity Index and Zeta Potential measurements

The hydrodynamic size, polydispersity index (PDI) and zeta potential (ζ -potential) of the AuNPs were analyzed using a Malvern Zetasizer Nano-ZS90. To determine the hydrodynamic size and PDI, 1 mL of the AuNPs was placed into 10 mm o.d. square polystyrene cuvette and the content was analyzed at 25 °C using dynamic light scattering (DLS). For ζ -potential measurements, 0.7 mL of the AuNPs was transferred into a disposable folded capillary cell and then analyzed at a voltage of 4 mV at 25 °C.

2.2.3.3 Transmission Electron Microscopy and Energy dispersive x-ray analysis

The AuNPs were centrifuged at 14000 rpm at 25 °C for 30 min, resuspended into 1 mL of deionized H_2O (dH_2O) and sent for Transmission Electron Microscopy (TEM) analysis (Department of Physics, University of the Western Cape). The sample solution was prepared by drop-coating one drop of the sample solution onto a carbon coated copper/nickel grid. The sample solution was then dried under a xenon lamp for 10 min and analyzed by the High-Resolution TEM. Transmission electron micrographs were collected using an FEI Tecnai G2 20 field-emission gun (FEG) TEM, operated in bright field mode at an accelerating voltage of 200 kV. Energy dispersive x-ray spectrum (EDX) was collected using an EDAX liquid nitrogen-cooled lithium doped silicon detector. The core diameter of the AuNPs was calculated by measuring the circumference of individual particles in the TEM micrographs using Image J software.

2.2.4 Functionalization of ssDNA aptamer probe to AuNPs

2.2.4.1 Conjugation and characterization of the apt-AuNPs

For conjugation, 5 μL of thiolated RBA-2 aptamer at different concentrations (25, 50, 75 and 85 μM) was stabilized with 1 μL of 10 mM TCEP, and incubated for 1 hr at 25 $^{\circ}\text{C}$, shaking at 650 rpm. Following incubation, 0.5 mL of prepared AuNPs was added to the thiolated RBA-2, in each tube and the mixture was left to incubate for 16 hrs at 25 $^{\circ}\text{C}$, shaking at 650 rpm. Subsequently, the mixture was aged (by adding 10 μL for every 20 min) with 50 μL of 1 M NaCl and 5 μL of 500 mM Tris-acetate buffer (pH 8.2). The mixture was further incubated for 24 hrs under the same conditions. Thereafter, the apt-AuNPs conjugates were characterized by measuring the absorbance spectra, size, PDI and ζ -potential as previously described in **Section 2.2.3.1** and **2.2.3.2**. The apt-AuNPs colour change was detected by visual observation. The unconjugated aptamers were removed by centrifuging the sample mixture at 10 000 rpm for 20 min at 4 $^{\circ}\text{C}$ and resuspending the pellet in 250 μL of dH_2O (three times). The apt-AuNPs conjugates were concentrated by centrifuging using the above conditions and resuspended in 30 μL of dH_2O . The apt-AuNPs conjugates were then characterized by the UV-vis spectrophotometer (as previously described in **Section 2.2.3.1**) and the concentration of the unconjugated aptamers for each sample was quantified using Qubit assay according to the manufacturer's protocol (Invitrogen, 2010).

2.2.4.2 Conjugation and characterization of the apt-AuNPs (Large scale)

For conjugation, 10 μL of 5'-thiolated RBA-2 aptamer (50 μM) was stabilized with 2 μL of 10 mM TCEP, and incubated for 1 hr at 25 $^{\circ}\text{C}$, shaking at 650 rpm. Following incubation, 1 mL of prepared AuNPs was added to the thiolated RBA-2 and the mixture was left to incubate for 16 hrs at 25 $^{\circ}\text{C}$, shaking at 650 rpm. Subsequently, the mixture was aged (by adding 10 μL for every 20 min) with 100 μL of 1 M NaCl and 10 μL of 500 mM Tris-acetate buffer (pH 8.2). The mixture was further incubated for 24 hrs under the same conditions. The unconjugated aptamers were removed by centrifuging the sample mixture at 10 000 rpm for 20 min at 4 $^{\circ}\text{C}$ and resuspending the pellet in 250 μL of dH_2O (three times). The apt-AuNPs conjugates were concentrated by centrifuging using the above conditions and resuspended in 30 μL of dH_2O . The experiment was done eight times and the 30 μL of the apt-AuNPs from each tube were combined to make a final volume of 240 μL . Thereafter, the apt-AuNPs conjugate was evaluated and characterised by the Cary 100 Bio UV-vis spectrophotometer

(scan from 200 nm to 800 nm) and by gel electrophoresis. The gel was performed using ultra low pure agarose gel (1%) in 1× TBE buffer and ran for 20 min at 120 V. The gel was stained with 3 μL of GelRed and the UVP Trans-illuminator and a camera phone were used to take images for analysis. The experiment was repeated using biotinylated RBA-2/15 mer' poly-T.

2.2.5 Preparation and evaluation of the LF test strips

To prepare the lateral flow test strips, HF180 nitrocellulose membrane, and the absorbent pad (composed of cotton litter fibers grade 320) were used. The test line was prepared by drawing a line with a yellow micropipette tip containing 12 μL of a pre-incubated (15 min at 25 °C) mixture of 1.7 mg/mL of streptavidin and 100 μM of the biotinylated RBA-1 in 1× PBS buffer. The control line was prepared by drawing a line with a yellow micropipette tip containing 12 μL of RBP4 (0.5 mg/mL) in 1× PBS buffer. Subsequently, the membrane was allowed to dry at 25 °C for 1 hr, followed by blocking with 1% w/v skimmed milk powder and 0.1% v/v empigen detergent in PBS-Tween20 (pH 7.4) for 15 min. The membrane was left to dry overnight, at 25 °C. The test strips were then cut into strips of 4 mm wide. Then, 5 μL of the RBA-2-AuNPs prepared in **Section 2.2.4.2**, was mixed with 10 μL of 1× SELEX buffer. The mixture was incubated for 10 min at 25 °C before being wicked onto the test strip. A Smartphone camera was used to take an image of the test strip. The experiment was repeated following the above protocol with slight modification: A) 2 mg/mL of the RBP4 protein was immobilized on the control line; B) the biotinylated poly-A aptamer was immobilized on the control line and 2 mg/ml of the RBP4 was immobilized on the test line. The thiolated RBA-2/15' mer poly-T was used for this experiment.

2.2.6 Development of a colorimetric aptasensor

2.2.6.1 Optimization of the aptamer and NaCl concentration

For aptamer and NaCl concentration optimization, a total of 200 μL of different concentrations of the biotinylated RBA-2/15' mer poly-T was added to 360 μL of AuNPs in different 1.5 mL tubes (final aptamer concentration: 0, 25, 50, 75 and 100 nM). The tubes were vortexed, followed by incubation at 25 °C for 30 min. A total of 75 μL of the apt-AuNPs was added to a 96-well microtiter plate, followed by the addition of different concentrations (0, 20, 40, 60, 80 and 100 mM) of NaCl. The samples were incubated at 25 °C for 5 min. The UV-vis spectra were measured using the SpectraMax 340PC384 and the absorption ratio A_{620}/A_{520} was calculated to determine the aggregation kinetics.

2.2.6.2 RBP4 detection based on colorimetric technique

For this experiment, 450 μL of AuNPs and 225 μL of 100 nM biotinylated RBA-2 /15' mer poly-T solution were added into a 1.5 mL tube, mixed and incubated at 25 $^{\circ}\text{C}$ for 30 min. Subsequently, 75 μL of the apt-AuNPs was added into 1.5 mL tubes. Then, 25 μL of different concentrations of RBP4 protein (0, 7, 15, 31, 62, 125, 250 nM) were added into the apt-AuNPs conjugate, mixed thoroughly, and incubated for another 15 min under the same conditions. The apt-AuNPs-RBP4 was transferred into their respective wells on a 96 well microtiter plate and 5 μL of 1 M NaCl solution was added to the wells. The absorbance of the above solutions at 520 nm and 600 nm were recorded using a SpectraMax 340PC384. The experiment was performed in duplicate and the average absorbance was calculated and used for the standard curve.



CHAPTER 3: RESULTS AND DISCUSSION

3.1 Secondary structure predictions of the selected aptamers

The aptamer secondary structure prediction plays a vital role in binding to the target because different folds allow the aptamer to exploit various binding mechanisms. Aptamers assume their structures upon binding to their target through a “lock and key” mechanism whereby they organise themselves to fit to the target. This allows aptamers to bind to their target with a greater specificity and affinity (Gold *et al.*, 1995, Eaton *et al.*, 1995). For this reason, it is absolutely necessary to evaluate the secondary structures of the aptamers in order to have a better understanding of their versatility. This analysis was carried out using M-Fold mapper.

The M-fold program predicted multiple secondary structures for RBA-1 (**Appendix A**); whereas, RBA-2, RBA-3 and RBA-4 had only one structure (**Figure 3.1** and **3.2**). However, only one predicted structure of RBA-1 will be reported in this study as it is assumed to be the most stable structure due to having the lowest minimum free energy. The predicted structures of all aptamers contained random region sequences and both the forward and reverse primers. The primer sequences are highlighted in colours whereby the green colour represent the forward and the blue colour represent the reverse primer. Looking closely at the predicted structures, it was apparent that both primers were involved in the formation of part of the stem-loop structures on RBA-1, RBA-3 and RBA-4, whereas, only the reverse primer was involved in the formation of part of a stem loop on RBA-2. Interestingly, RBA-1 showed to have a bulge composed of -CAG- at base 5-7 which is not observed on other aptamer structures (**Figure 3.1**). Furthermore, a stem-loop composed of -TAGTAAGTGCAA- was present at base 62-73 for all four predicted structures, which is a component of the reverse primer (highlighted by the red boxes). Although the primer regions are involved in the formation of the secondary structure, they are not expected to have recognition sites. However, these stem-loops may play an ancillary role in the binding of these aptamers to the target protein.

The results in the present study indicated that RBA-1 and RBA-3 shared a conserved motif of -GTTG- at base 44-47; whereas, RBA-1 and RBA-2 shared a motif of -AGGGG- at base 26-32. This provided a possibility of these aptamers binding to RBP4 with a higher affinity. Qin *et al.* (2013) previously reported that conserved motifs which are often located in stem-loop structures are most likely to be responsible for aptamer binding to the target.

The results further revealed that RBA-3 had the lowest minimum free energy ($\Delta G = -5.48 \text{ kJ mol}^{-1}$). Therefore, this aptamer may be highly stable and may have a high binding affinity as compared to other aptamers. RBA-1 and RBA-4 had relatively similar structures; however, RBA-4 ($\Delta G = -4.35 \text{ kJ mol}^{-1}$) had the second lowest minimum free energy while RBA-1 ($\Delta G = -2.37 \text{ kJ mol}^{-1}$) had the highest minimum free energy. The minimum free energy of RBA-1 was comparable with that of RBA-2 ($\Delta G = -2.84 \text{ kJ mol}^{-1}$). despite having slightly different structures. Li *et al.* (2015) have isolated four ssDNA aptamers (Q2, Q3, Q4 and Q5) of which the M-fold results revealed that all aptamers contained stem-loop structures, with Q4 exhibiting the lowest minimum energy value of $-25.14 \text{ kJ mol}^{-1}$.

Even though we have assumed that RBA-3 will bind to the RBP4 with a higher affinity, it was also possible that the non-binding domain may interfere with the interaction between the aptamer and target protein by formation of complex secondary structures, which in turn may inhibit the binding domain to fold into the desired confirmation for binding the target. In order, to validate the binding affinity and specificity of these aptamers, kinetic studies were used.



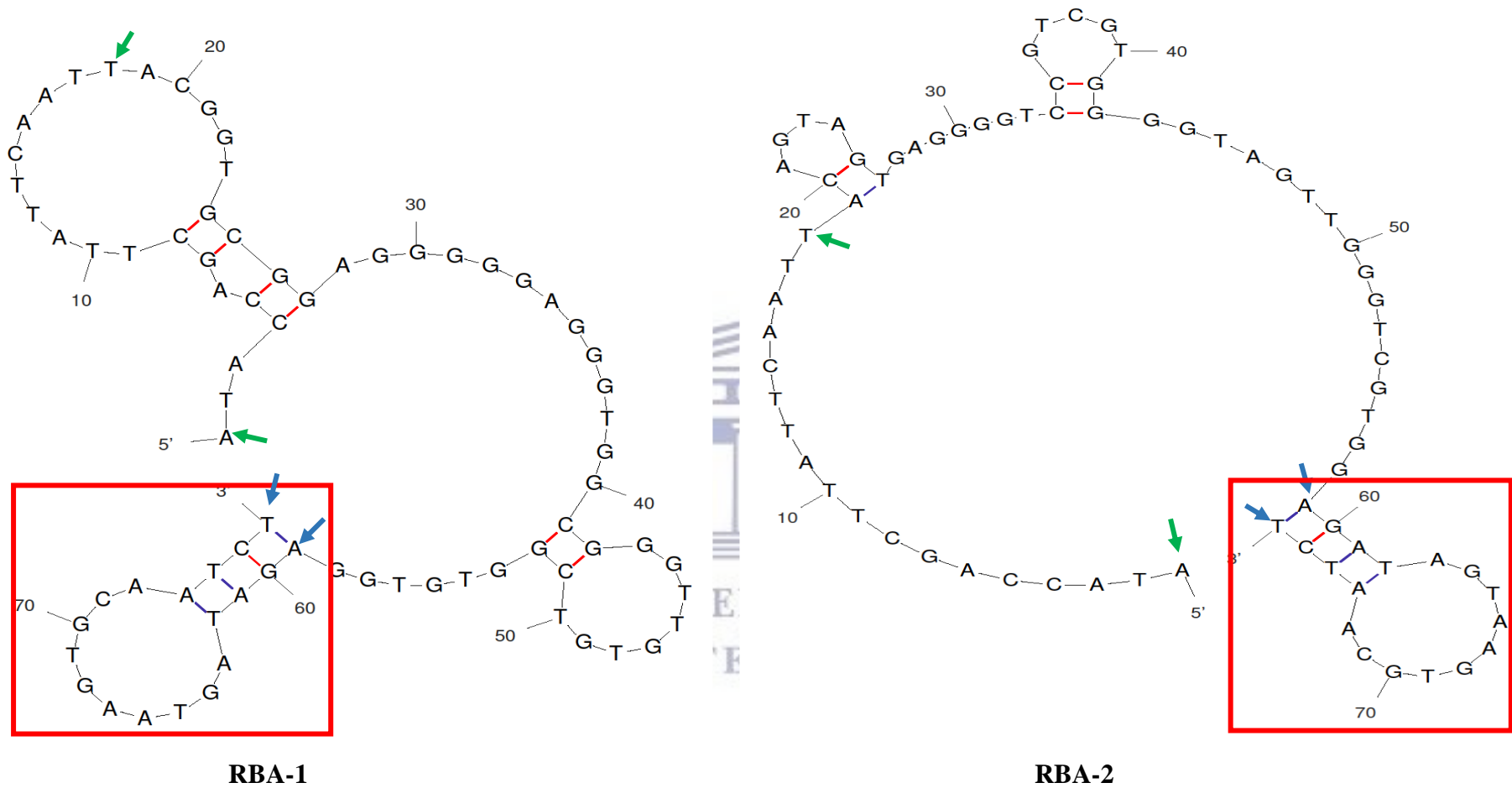


Figure 3.1: Secondary structure prediction of RBA-1 ($\Delta G = -2.37 \text{ kJ mol}^{-1}$) and RBA-2 ($\Delta G = -2.84 \text{ kJ mol}^{-1}$) as predicted by the M-fold program. The ΔG represents the minimum free energy of each aptamer. The forward primer sequence (base 1-18) is shown by the green colour and the reverse primer (base 59-76) are shown by the blue colour. Common stem loops within each aptamer are depicted using red boxes.

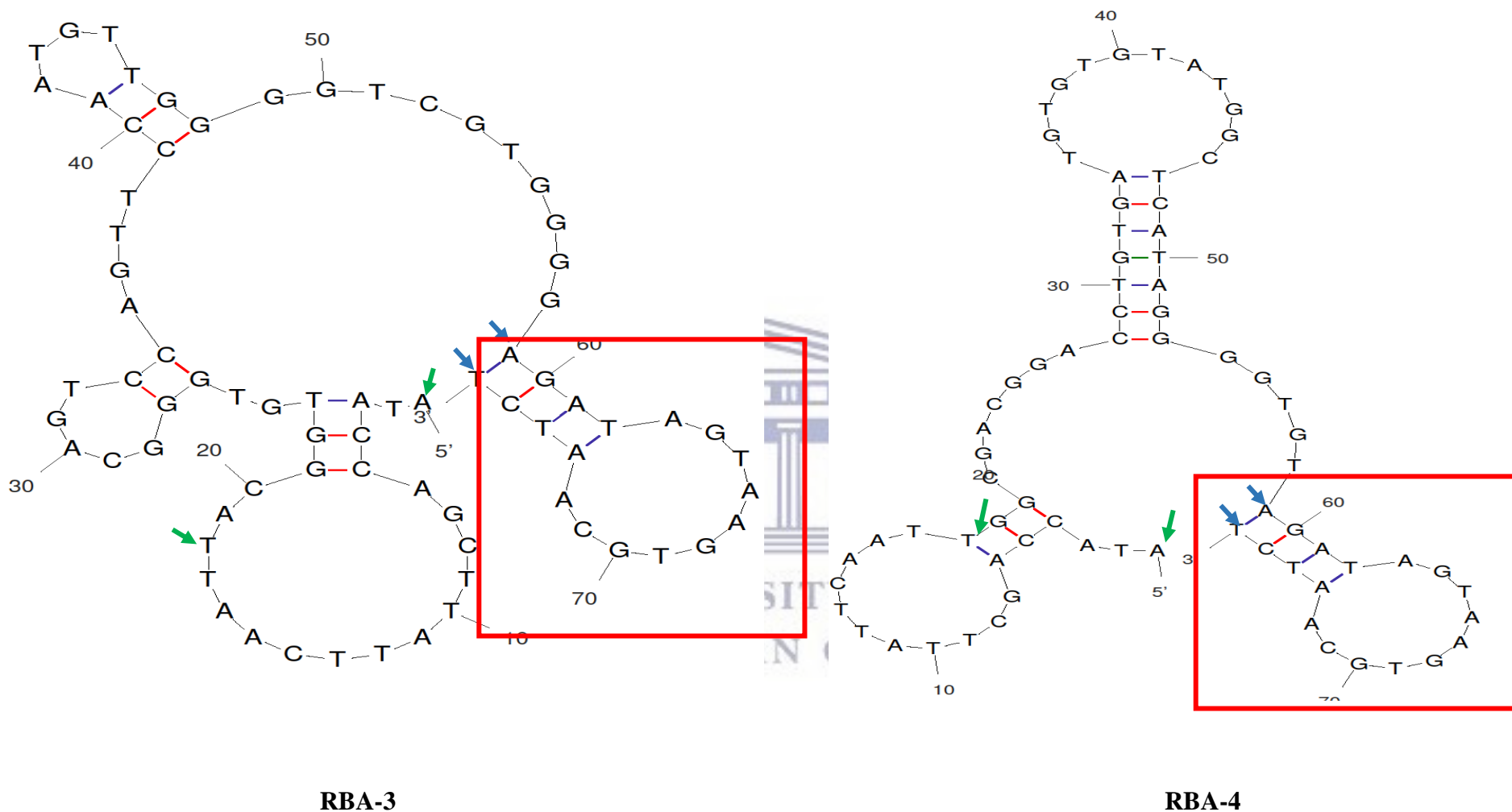


Figure 3.2: Secondary structure prediction of RBA-3 ($\Delta G = -5.48 \text{ kJ mol}^{-1}$) and RBA-4 ($\Delta G = -4.35 \text{ kJ mol}^{-1}$) as predicted by the M-fold. The ΔG represents the minimum free energy of each aptamer. The forward primer sequence (base 1-18) is shown by the green colour and the reverse primer (base 59-76) are shown by the blue colour. Common stem loops within each aptamer are depicted using red boxes.

An alternative way of predicting secondary structure is by analyzing the G-quadruplex of the aptamers. G-quadruplexes are usually formed in the presence of a guanine-rich nucleotide sequence in a square planar array. Each G-quadruplex is then assigned a G-score which can be defined as the probability of the aptamer and the number of guanines present to form Quadruplex forming G-Rich Sequences (QGRS) (Viglasky and Hianik, 2013). For the present study, the predictions of the G-quadruplex secondary structures were made computationally using a QGRS Mapper.

The results obtained in this analysis demonstrated that RBA-1, RBA-2 and RBA-3 were able to form G-quadruplexes with G-scores of 21, 18 and 3, respectively (**Table 3.1**). On the other hand, RBA-4 was not able to form the G-quadruplex structures; however, this was acceptable because not all aptamers are able to form/contain such structures. The number of bases responsible for forming G-quadruplex structure for RBA-1 was 14 nucleotide's (nts), starting at position 31 on the sequence of 76 nts full length aptamer sequence. RBA-2 had 28 nts also starting at position 31; whereas, RBA-3 had 30 nts starting at position 21 of the full length aptamer sequence. Furthermore, RBA-1 and RBA-2 had the highest G-Scores of 21 and 18, respectively. This indicates that both aptamers had a higher number of guanines which are responsible for forming QGRS secondary structures. In addition, these aptamers were also stable. This is because the importance of G-quadruplexes lies in the stability of their 3D aptamer structure and in the improvement of electrostatic interactions to the positively charged binding sites on the ligands. This is mostly attributed to the fact that the negative charge density of G-quadruplexes is twice as high as that of linear DNA (Gatto *et al.*, 2009). Using the same software, an independent study by Espiritu *et al.* (2018) identified three aptamers (AP65A1, AP65A3 and AP65A6) that had a G-score of more than 20, indicating a high probability of forming G-quadruplexes.

Table 3.1: G-quadruplex structure of the aptamer.

Aptamer ID	Position	Length	QGRS	G-Score
RBA-1	31	14	<u>GGGAGGGTGGCGGG</u>	21
RBA-2	31	28	<u>GGTCCGTCGTGGGTAGTTGGGTCGTGG</u>	18
RBA-3	21	30	<u>GGTGTGGGCAGTCCAGTTCCAATGTTGGGG</u>	3
RBA-4	0	0	N/A	0

3.2 Evaluation of the binding affinity of the selected aptamers

Evaluating the kinetics of these aptamers allow the understanding of how rapidly the aptamers and RBP4 associate and also how soon the aptamer-RBP4 complex dissociates. It is well documented that the tighter the bond of the aptamer ligand, the lower the dissociation constant (K_D) will be. Therefore, an ideal aptamer would have a fast association rate but a slow dissociation rate, resulting in an aptamer-ligand complex maintained for longer, subsequently leading to a lower equilibrium K_D . In regards to the above statement, it is assumed that a low K_D shows higher binding affinity (Stoltenburg *et al.*, 2007). And since PoC tests are desired to be fast and accurate, low nM and pM values are preferred ranges which allows binding in seconds to minutes only (Svobodová *et al.*, 2012).

3.2.1 Binding of aptamers to RBP4 by SPR

For this study, aptamer interactions were evaluated in real time using the Biacore 3000 SPR instrument. SPR is a phenomenon that happens on the surface of a metal film when the incident light is polarized parallel to the plane of incidence. The electron-plasmon oscillation generates the evanescent electromagnetic field that penetrates the metal film into the sample solution near the film. By fixing the light source and the metal film, the change in the angle of the reflected light is related only to the refractive index of the sample solution near the film (Homola, 2008). The resonance signal is related linearly to the analyte immobilized at a broad concentration range (Zhu *et al.*, 2015, Drescher *et al.*, 2009).

The target protein (RBP4), was immobilized on the CM5 sensor chip, to allow for subsequent aptamer binding (**Figure 3.3**). Four channels were used in this study, the first channel was activated with EDC/NHS, the second channel was allotted for immobilization of the RBP4 and the third channel was used as control (IgG) and the fourth channel was blocked with EDC/NHS. When the protein was immobilized on the chip, there was interaction between the His-tagged RBP4 via the amino group on the surface of the chip. The association followed a single exponential curvature until it reached equilibrium. When the surface of the chip became saturated, an association constant was observed. IgG was used as the counter protein; thus, it was immobilized in the same manner as above. After immobilization of the two proteins on the surface, the four aptamers were injected in their respective channels on the sensor chip to investigate their binding affinities. The aptamers were injected at different

concentrations, at a constant flow rate. The binding affinities of the aptamers to RBP4 were measured by the changes in the resonance unit.

Figure 3.4 shows that the response units increased with the sampling time and reached the steady value at 700 s. According to the results, RBP4 bound to the aptamer with a fast association rate constant and the relative response return to the baseline at 450 s after sample injection. RBA-1 at 10 μM gave a response unit (RU) of 327, while RBA-2, RBA-3 and RBA-4 at 1 μM had a RU of 153, 147 and 91, respectively. The sensorgrams also indicated that the dissociation curve did not show any decrease; thus, indicating that there was a tighter binding of the aptamers to RBP4.

The K_D of the aptamers was estimated using the Langmuir 1:1 model, with a range of concentrations (10 - 40 nM). This model is the simplest and most widely used in literature (Chang *et al.*, 2014; Kaur and Yung; 2012). The obtained sensorgrams showed specific shift at the beginning of association phase in majority of curves which complicated the fitting. This specific shift in the sensorgram may be attributed to the presence of 0.02% Tween which was part of the constituents in the binding buffer. Hence, for the calculation of K_D , different selections for fitting (part of association and dissociation curve) were used and resulted in different K_D values.

Based on the selections used, a good fit to the Langmuir 1:1 model was obtained for RBA-1, RBA-3 and RBA-4, as demonstrated by the χ^2 (χ^2) values (**Table 3.2**). The χ^2 is a statistical measure of closeness of fit of experimental data to the theoretical model used to determine the K_D . It describes how well the results agree with the curve-fitting of the model used. The χ^2 values lower than the noise RU (in this case, ~ 20 RU), indicate a good fit. Therefore, for kinetic evaluations, the results were found to be within acceptable ranges of the relevant statistical measures (Gopinath, 2010). However, RBA-2 displayed a kinetic parameter that does not fit the Langmuir 1:1 model used for analysis. This is sometimes experienced as SPR-based kinetic evaluations can be affected by several factors such as the purity of reagents, the immobilization procedure and level, ligand activity, flow rate and analyte concentration range (Gopinath, 2010). However, the encountered problem could not be attributed to the above factors as the aptamers were injected over the same ligand surface using the same immobilization procedure. Therefore, it can be hypothesized that the

conditions in which the binding reactions took place were much suitable for the other three aptamers and may be unfavorable for RBA-2.

The results further demonstrated that all four aptamers had a higher binding affinity for RBP4. RBA-1, RBA-2 and RBA-4 had K_D values within a nM range and RBA-3 showed a K_D value within a pM range; which are the preferred ranges for aptamer-protein interactions (**Table 3.2**). O'Sullivan and her team were able to select an aptamer that bind with a high affinity to *Trichomonas vaginalis* Adhesion protein. This aptamer (AP65_A1) had a K_D value of 56 nM and a χ^2 value of 3.21 which indicated a good fit to the Langmuir 1:1 model (Espiritu *et al.*, 2018).

Interestingly, the present study has shown that RBA-2 exhibit a dissociation constant of 3.74 nM which is much lower than that of the reported K_D value of RBA-2 ($K_D = 0.2 \pm 0.03 \mu\text{M}$) by Lee *et al.* (2008). In the present study, RBA-2 showed higher affinity to RBP4 which may be attributed to the modification introduced at the 5' end. It is common to see such differences in the binding affinities of aptamers free in solution and immobilized, as the immobilization process may obstruct the folding of the aptamer into its optimum 3D structure for target binding. This is often resolved by using spacers to extend the aptamer from the surface and facilitate its 3D formation optimum target binding (Espiritu *et al.*, 2018). An independent study investigated how the immobilization orientation of the aptamers affects their functionality in SPR measurements. The study demonstrated that the immobilization of aptamer (PA#2/8) at its 5' end resulted in low binding affinity to the target protein (Protein A). However, a high binding affinity of the aptamer to Protein A was observed with a 3' end immobilized aptamer. This indicated that a free 5' end of the aptamer was necessary for its correct folding as basis for formation of the binding complex with the target (Stoltenburg *et al.*, 2015). In contrast to the study by Stoltenburg *et al.* (2015), the present study showed that a 5' end immobilized aptamer resulted in high binding affinity of the aptamer to the target.

Furthermore, to corroborate the statements made above regarding the binding affinities of these aptamers, the intrinsic relationship between the affinities and structures were investigated. Aptamers were compared with regards to their binding affinities and secondary structures. The results revealed that the aptamer (RBA-3) with the highest binding affinity had a complex structure with an extra stem-loop (**Figure 3.1**). This indicated that the closeness of the loops did not affect the binding affinity of this aptamer to the target.

Moreover, this aptamer had the lowest minimum free energy, indicating that it was more stable; hence, it was not surprising that it had a higher binding affinity to RBP4. Interestingly, despite a huge difference of minimum free energies between RBA-4 and other two aptamers (RBA-1 and RBA-2) and also their structures, there was no significant difference in their binding affinities.

IgG was used as a control to conclusively confirm aptamer selectivity to the target protein. The results demonstrated that all the aptamers had a high binding affinity to RBP4 whilst having no interaction with IgG. This suggested that the aptamers used in this study were only specific to RBP4. A previous study used adiponectin, visfatin, bovine serum albumin and human serum albumin proteins as counter targets to evaluate the aptamers' specificity. Their study revealed that RBA-1, RBA-3 and RBA-4 were not specific to RBP4; thus, they were not considered for further characterization (Lee *et al.*, 2008). A second study by the same group also showed that RBA-2 was only specific to RBP4 (Lee *et al.*, 2012); thus, making this aptamer a good candidate for downstream applications due to its specificity.

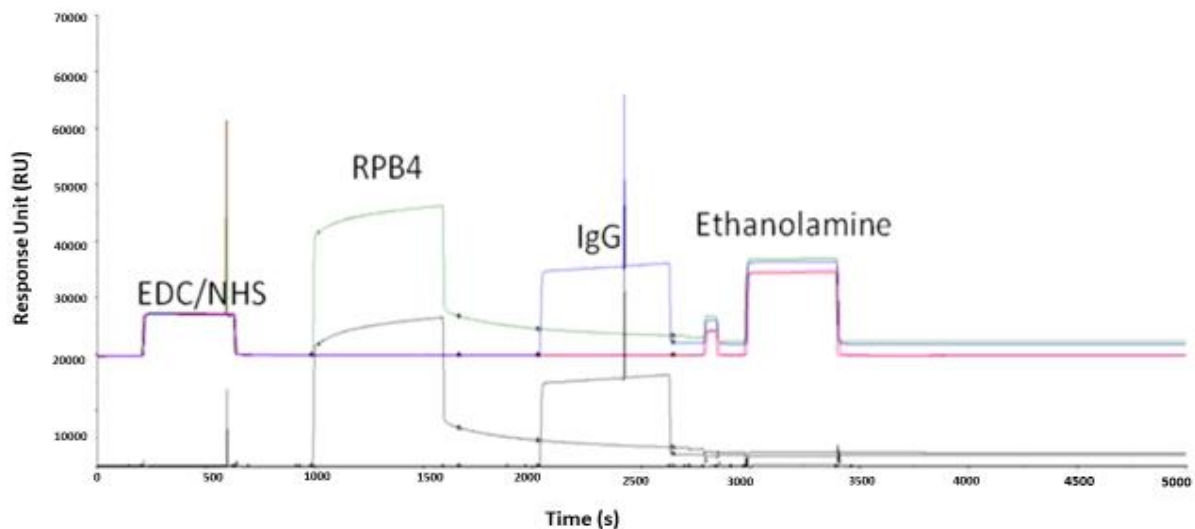


Figure 3.3: Representative sensorgram for the coupling of RBP4 on an SPR sensor chip surface. RBP4 and IgG were immobilized using amine coupling chemistry. Activation of the sensor chip was achieved by injecting the EDC: NHS over the surface of the chip to activate the carboxyl groups of the ligand. Activated carboxyl groups which had no proteins bound were then blocked with ethanolamine. The surface was regenerated and unbound proteins were removed with 2 M NaCl + 50 mM NaOH.

Table 3.2: Affinity dissociation constant of the candidate aptamer by SPR.

Aptamer ID	K_D	Chi²
RBA-1	3 nM	6.2
RBA-2	3.74 nM	33.9
RBA-3	2.52 pM	1.71
RBA-4	3.65 nM	15.7



UNIVERSITY *of the*
WESTERN CAPE

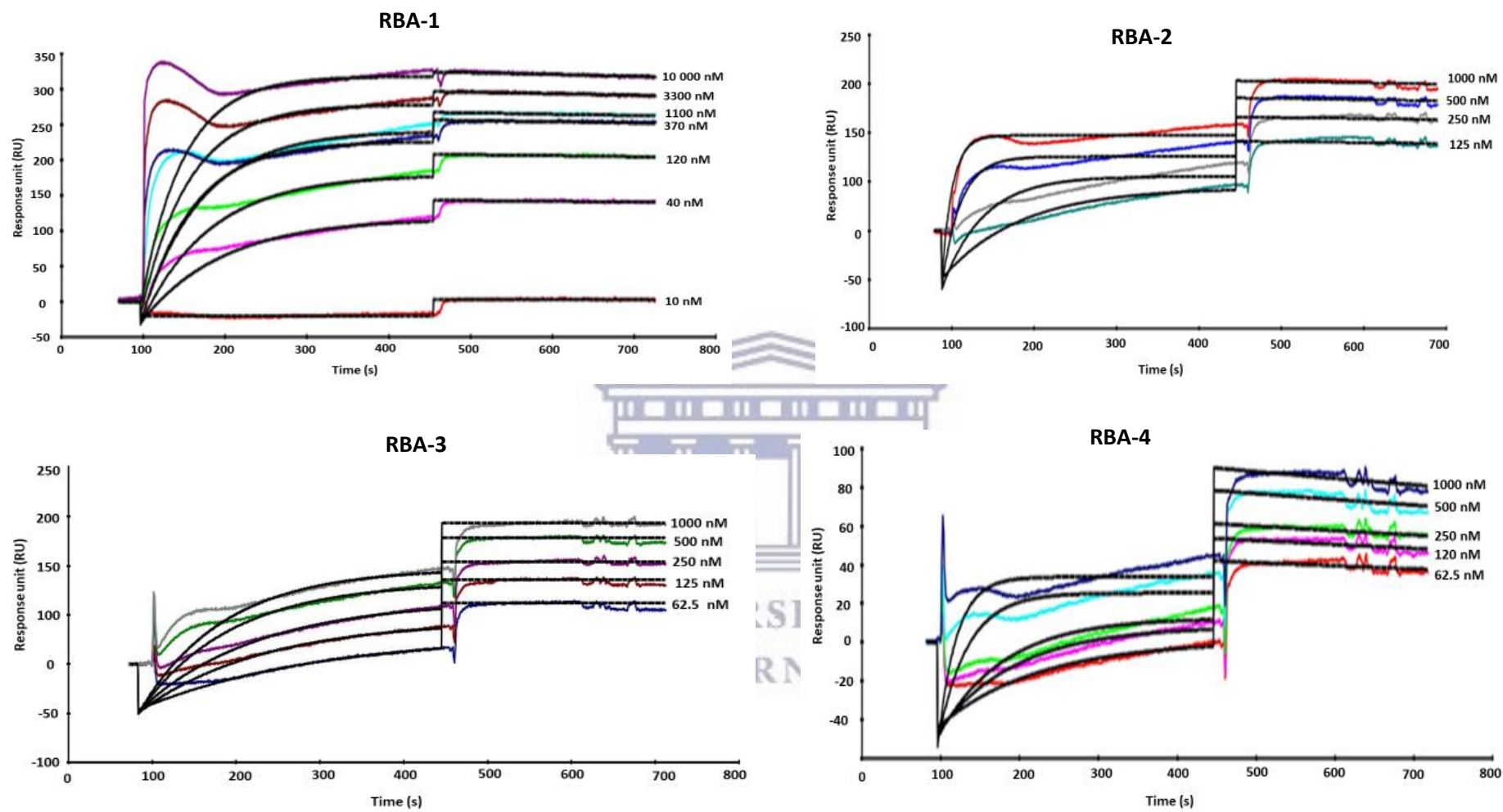


Figure 3.4: Measurement of the interaction of aptamers with RBP4 by SPR. Dissociation constants for the selected aptamers immobilized on a CM5 sensor chip were determined by SPR. Data are presented as real-time graphs of response units against time and were evaluated using BIAevaluation 3.0 software (Biacore).

3.2.2 Binding of aptamers to RBP4 by EMSA

To further confirm the interaction of the protein and the selected aptamers, an electrophoretic mobility shift assay (EMSA) was employed. EMSA is a rapid and a sensitive method for the detection of protein-nucleic acid interactions. It is based on the principle that a nucleic acid bound to the target protein will migrate slower through a gel matrix than the free nucleic acid. This technique is used for qualitative purposes; however, under suitable conditions, it can also be employed to provide quantitative data for the determination of binding stoichiometry, affinities and kinetics (Hellman and Fried, 2007).

For this study, RBA-1 and RBA-2 were selected to validate their interaction with RBP4. The selection of RBA-2 was based on the results published from a previous study which demonstrated RBA-2 was specific to RBP4 (Lee *et al.*, 2008); whereas, the selection of RBA-1 was based on the secondary structure prediction analysis. As shown in **Figure 3.5**, there were bands appearing near the 75 bps band, which corresponds to the free aptamer. The migration of the band produced for RBA-1/RBP4 was much slower than the migration of the band produced for the free RBA-1. This suggested that RBA-1 was able to interact/bind with RBP4; thus, validating the results obtained from the SPR analysis. However, the same shift was not observed with RBA-2/RBP4. This could be attributed to rapid dissociation during electrophoresis which prevented detection of complexes or slow dissociation which resulted in underestimation of binding density. It was postulated that the His-tag modification on the target protein might also be preventing the aptamers from binding. In addition, the control (lane 6) had a band at around 200 bps which was also found in the protein/aptamer complex suggesting that the band could have formed during the refolding of the aptamer.

Based on the results from the previous experiment, a second experiment was performed with different concentrations of RBP4 incubated with a fixed concentration of the RBA-1. As shown in **Figure 3.6**, there were bands appearing near the 75 bps band which corresponded to the free RBA-1. There were also bands obtained on top of the wells which were associated with the aptamer/protein complex; however, the same effect was observed in lane 1 (RBA-1 only); thus, suggesting that the bands were not due to the slow migration of the protein/aptamer complex. Therefore, the results obtained by EMSA analysis did not provide conclusive evidence of molecular interaction and must be done in combination with other methods.

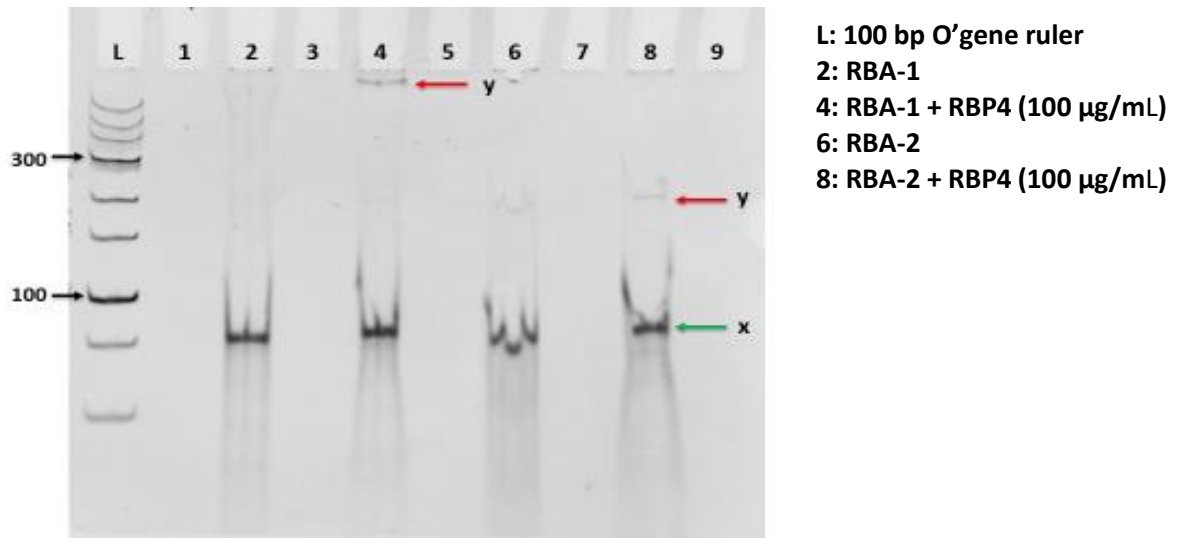


Figure 3.5: Evaluation of RBP4 binding to RBA-1 and RBA-2 aptamers using EMSA. RBP4 was incubated in 100 mg/mL of aptamers for 30 min, the samples were electrophoresed in a native polyacrylamide gel. The red arrow (y) indicate the migration of the aptamer/protein complex, while the green arrow (x) indicate the migration of the free aptamers.

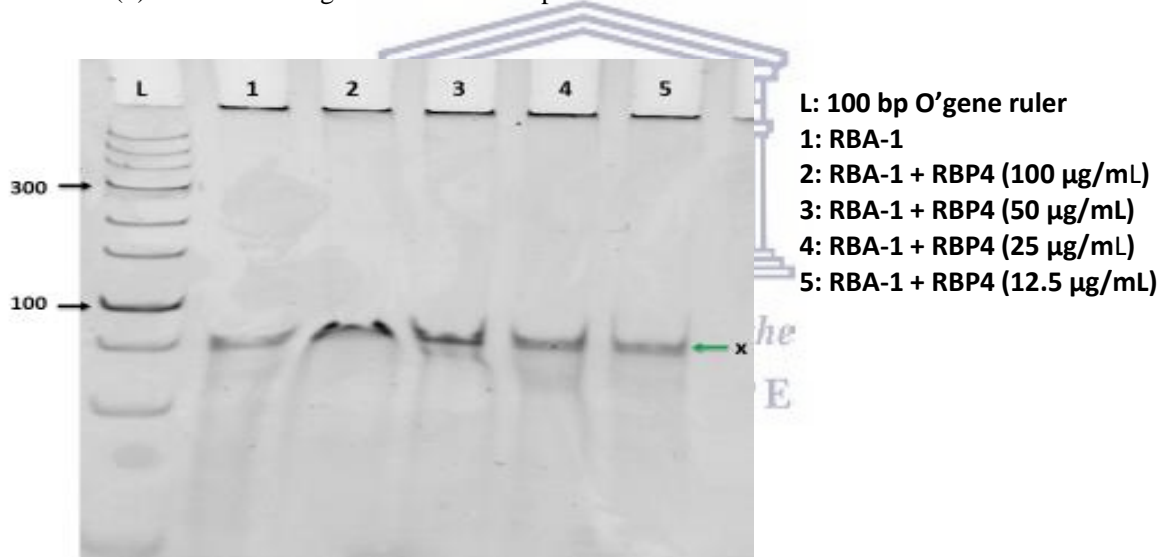


Figure 3.6: Evaluation of RBP4 binding to RBA-1 aptamer using EMSA. RBP4 was incubated in different aptamer concentrations for 30 min, the samples were electrophoresed in a native polyacrylamide gel. The green arrow (x) indicate the migration of the free aptamers.

3.2.3 Binding of aptamers to RBP4 by ELAA

Due to the inconclusive results obtained using EMSA analysis, a direct enzyme linked aptamer assay was established to confirm the interaction between the two aptamers (RBA-1 and RBA-2) with RBP4, respectively. ELAA is a fundamental tool of immunological, medical, and biochemical research. It is based on the principle of target-aptamer interactions in combination with photometric visualisation of the binding results and is typically performed in microtiter plates (Stoltenburg *et al.*, 2016). The use of a plate-based ELAA is a generally rapid and a simple way to screen and characterize aptamer binding to protein targets.

Figure 3.7: A shows that when RBA-1 was immobilized, a slight increase in the signal was observed; however, there was also a signal in the control which was attributed to the background signal. The results were inconclusive and indicated that there was no interaction between RBA-1 and RBP4. However, **Figure 3.7: B** shows that when RBA-2/15 mer' poly-T was immobilized, an increased signal was obtained; and a negligible background signal was observed in the control (0 mg/mL). The results demonstrated that the RBA-2/15 mer' poly-T was able to bind to RBP4. The enhanced affinity of this aptamer to the protein may be attributed to the poly-T modification introduced at the 5' end. This is because the use of a spacer decreases steric hindrance resulting in a better folding and target recognition (Zhu *et al.*, 2011).

The results obtained by ELAA supported the results obtained by SPR analysis; however, the results demonstrated the use of spacers are required for ELAA. Using the same technique, Stoltenburg *et al.* (2016) evaluated the binding interaction between protein A aptamer and *Staphylococcus aureus*. Their study demonstrated that ELAA allowed a high affinity detection of Protein A by the aptamer as compared to other methods which were previously used for analysis and that the truncated 3'-biotinylated aptamer PA#2/8 showed the best binding features $K_D = 11.3 \pm 1.4$ Nm.

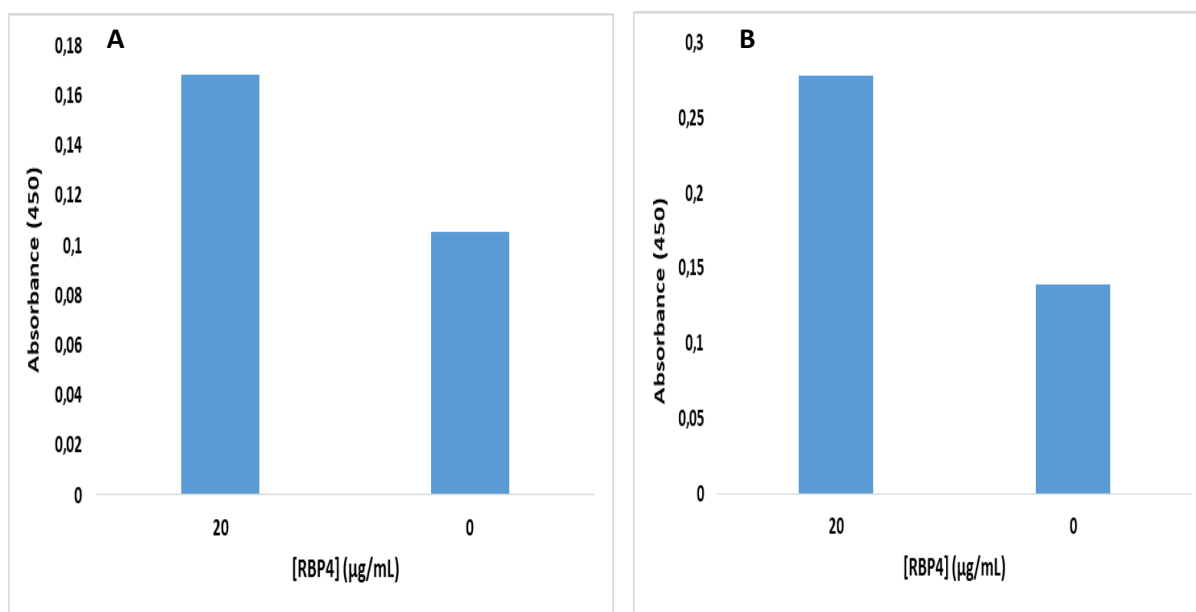


Figure 3.7: Evaluation of target binding of aptamer (RBA-1 and RBA-2) using ELAA. Protein solution of 20 µg/mL was used for coating the microtiter plates. 100 nM of 5'-biotinylated RBA-1 and of 5'-biotinylated RBA-2/15 mer' poly-T were added for binding (A and B), respectively. The blank reaction (0 µg/mL) represents the control without any protein coating.

3.3 Identification of dual aptamers

We further investigated the possibility of having dual aptamers that bind to two different sites of RBP4. The first mention of dual aptamers that bound to distinct sites of human thrombin was reported in 1997 by Tasset and colleagues (Tasset *et al.*, 1997). These thrombin dual aptamers have been used in several analytical techniques and diagnostic applications (Xu *et al.*, 2009). The biggest advantage of having dual aptamers is an easy and broad modification of the capture and reporter aptamers in order to enhance the detection of target in sensing platforms (Raston and Gu, 2015). Herein, two assays (SPR and ELAA) were used to evaluate the possibility of having two aptamers that bind to RBP4 at two different sites.

Due to the high specificity of RBA-2 as previously reported in **Section 3.2**, this aptamer was chosen as the capture aptamer. The SPR analysis showed that RBA-1 bound to RBA2-captured/immobilized RBP4 as indicated by an increase in the sensorgram. In contrast, there were no significant changes observed when RBA-3 and RBA-4 were injected into RBA2-captured/immobilized RBP4 (**Figure 3.8**). The results indicated that there was an interaction of RBA-2 and RBA-1 with RBP4; thus, suggesting that these dual aptamers bind distinctively to different sites on RBP4 protein. However, the results also indicated that the aptamers-RBP4 complex dissociate rapidly. In contrast, the lack of observed changes with RBA-3 and

RBA-4 suggested that they bind at the same site on RBP4 as RBA-2. However, it is possible that by reversing the immobilization and using RBA-3 and RBA-4, we could have found different interactions. Similarly, Ahmad Raston and Gu (2015), have successfully developed cognate dual aptamers for another diabetes biomarker (vaspin). Jauset Rubio *et al.* (2016) also reported on β -conglutin dual aptamers binding distinct sites. The SPR analysis in their study showed that two aptamers were able to bind to β -conglutin as indicated by an increase in the sensorgram when the full-length (β -CA I and β -CA II) were used.

In order to validate the obtained results, evaluation of the dual aptamer was performed using an ELAA. Once again, RBA-2 was used as a capture probe and was immobilized on the plate. RBP4 was incubated with the aptamers and the unbound was removed by washing. **Figure 3.9** shows that at 100 μ g/ml RBP4 concentration, RBA-1 showed a concentration dependent increase in signal. This suggests that with an increasing concentration of RBP4; RBA-1 and RBA-2 bound to RBP4, again validating the results obtained using SPR. In contrast, incubation with RBA-3 and RBA-4 did not increase the signal, further proof that they bind to same site as RBA-2. Using a similar method, dual aptamers that bind to platelet-derived growth factor B-chain homodimer (PDGF-BB) were conjugated to the surface of a green fluorescent ferritin nanoparticle (which functioned as a reporter aptamer) and the bottom of wells respectively for a sandwich ELISA. This aptamer-based ELISA was capable of detecting PDGF-BB at a concentration as low as 100 fM, with higher sensitivity than antibody-based ELISA due to the multivalency effect of aptamer-conjugated nanoparticles (Kim *et al.*, 2011). Li *et al.* (2018) also identified dual aptamers that bind distinctively to ronalite using ELAA. The aptamers were further used in the development of a sandwich LF test strips.

The results obtained in the current study supported that RBA-1 and RBA-2 indeed had different secondary structures (as shown by M-Fold) and that they bind at different sites of RBP4. Therefore, RBA-2 was selected as capture aptamer and RBA-1 as reporter aptamer for RBP4 detection in the development of the LF test strips.

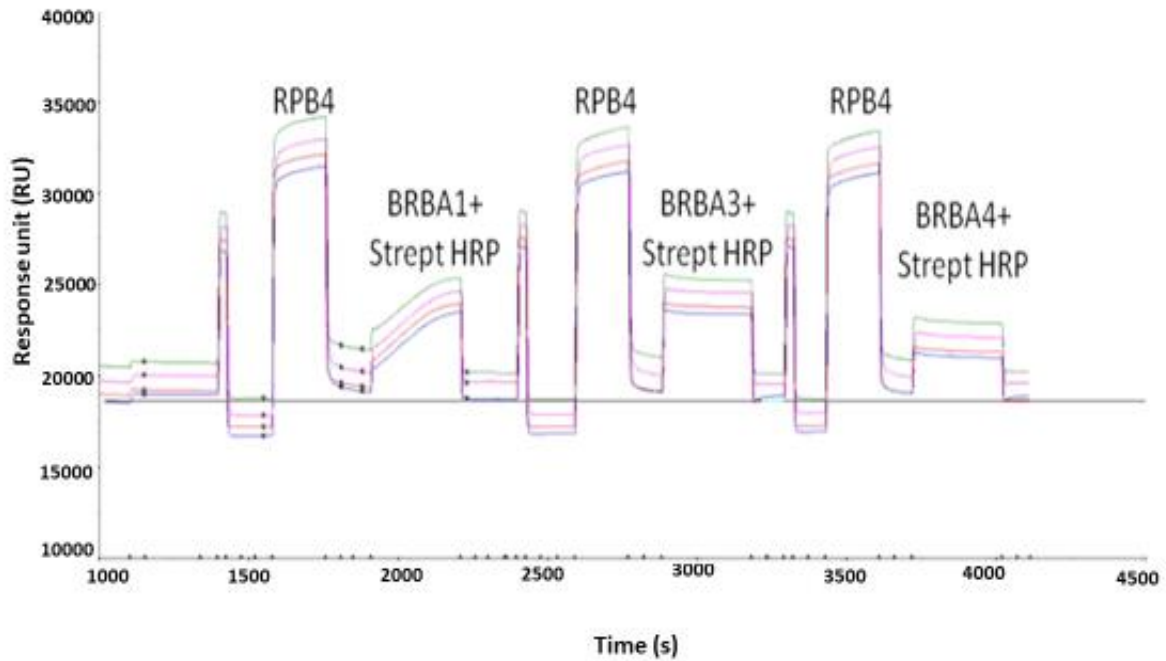


Figure 3.8: Dual aptamer based sandwich assay by SPR: the binding assays were performed using 10 μM thiol-RBA-2 as capture aptamer immobilized on gold sensor chip.

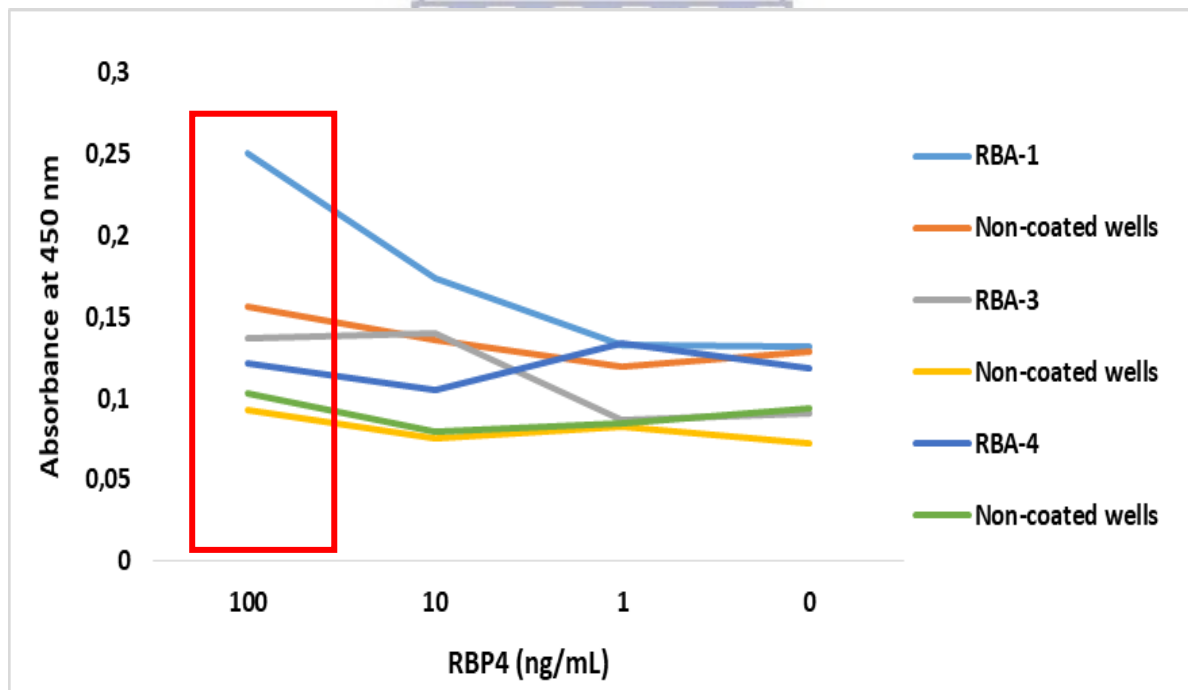


Figure 3.9: Dual aptamer based sandwich assay by ELAA: using 500 μM of thiol-RBA-2 immobilized on the plate, RBP4 (0 - 100 $\mu\text{g/mL}$) and 10 μM reporter aptamer (RBA-1, RBA-3 and RBA-4).

3.4 Synthesis and characterization of AuNPs

Recent advances in nanotechnology have provided a depth of insight and new opportunities for the application of nanomaterials in biological analysis and disease diagnosis (Matsui *et al.*, 2004; Saji *et al.*, 2010; Zhu *et al.*, 2004). These nanomaterials are usually integrated in various parts of existing sensing platforms in order to offer innovative detection systems (Quesada-González and Merkoçi, 2017). Among these sensing nanomaterials, AuNPs have been mostly used in the development of colorimetric biosensors due to their unique optical properties, strong SPR and high extinction coefficient in the visible wavelength spectrum/range (He *et al.*, 2008; Kim *et al.*, 2016; Lin *et al.*, 2005; Liu and Lu, 2004). In addition, they are highly stable and available in large quantities with controlled size and shape (Zhang *et al.*, 2012). Hence, their application has remarkably increased the speed and success of PoC testing. For this experiment, AuNPs were synthesized by using citrate reduction method (Sibuyi *et al.*, 2017) and characterized using UV-vis spectrophotometer, DLS, ζ -potential and TEM.

3.4.1 UV-vis spectrometry of AuNPs

UV-vis spectrometry is an important aspects of characterizing AuNPs. With increase in NPs size, the absorption spectra shift to longer wavelengths and the width of the adsorption spectra is related to the size distribution range. Generally, AuNPs display a single absorption spectrum between ranges of 510 - 550 nm with a bright ruby-red colour, which may vary depending on their size (Verma *et al.*, 2014). In this study, the absorption maximum (λ_{\max}) was observed at 517 nm, which indicated that the AuNPs were approximately 14 nm in size (**Figure 3.10**). The AuNPs had an absorbance value of 1,084 OD, and a concentration of 6.94 nM which is within the preferred concentration range for conjugation. The concentration of the AuNPs was calculated based on the formula:

$$C=A_{450}/\epsilon_{450}$$

Where: C = concentration, A₄₅₀ = absorbance at 450 nm, ϵ_{450} = molar extinction coefficient at 450 nm.

Furthermore, the absorption spectra of the AuNPs was sharp, thus indicating that the AuNPs were uniform and stable. Similar findings were reported on AuNPs of variable sizes between

13-20 nm with λ_{\max} around 520 nm (Agnihotril and Bhide, 2012; Liu *et al.*, 2010; Qadami *et al.*, 2018).

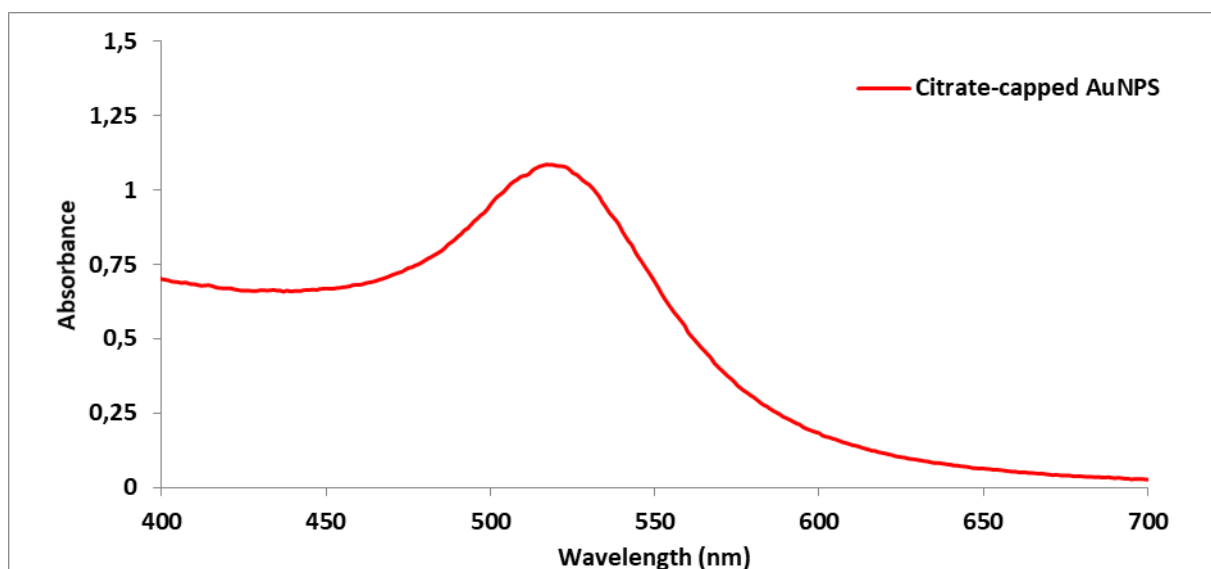


Figure 3.10: UV-vis spectrum of the citrate-capped AuNPs.

3.4.2 DLS and PDI analysis of the AuNPs

Hydrodynamic size of AuNPs was measured by DLS, which is one of the most preferred analytical methods for the characterization of AuNPs size. In the measurement, particles are exposed to a laser beam and the particles size is specified from the scattered light generated as a result, using the dependence of particles size on the spatial intensity and distribution pattern (Bhattacharjee, 2016)

As shown in **Figure 3.11**, the AuNPs had an average hydrodynamic diameter of 16.82 nm, which could be due to the hydrodynamic capacity of H₂O surrounding the AuNPs. About 97.8% of the AuNPs were within 17,93 nm and only 2.2% were about 5077 nm in size. This indicated that most of the AuNPs were of a smaller size. The PDI of the AuNPs was found to be 0.228, which indicated that the AuNPs were mostly monodispersed.

	Size (d.nm):	% Intensity:	St Dev (d.nm):
Z-Average (d.nm): 16,82	Peak 1: 17,93	97,8	6,034
Pdl: 0,228	Peak 2: 5077	2,2	584,1
Intercept: 0,927	Peak 3: 0,000	0,0	0,000

Result quality : Refer to quality report

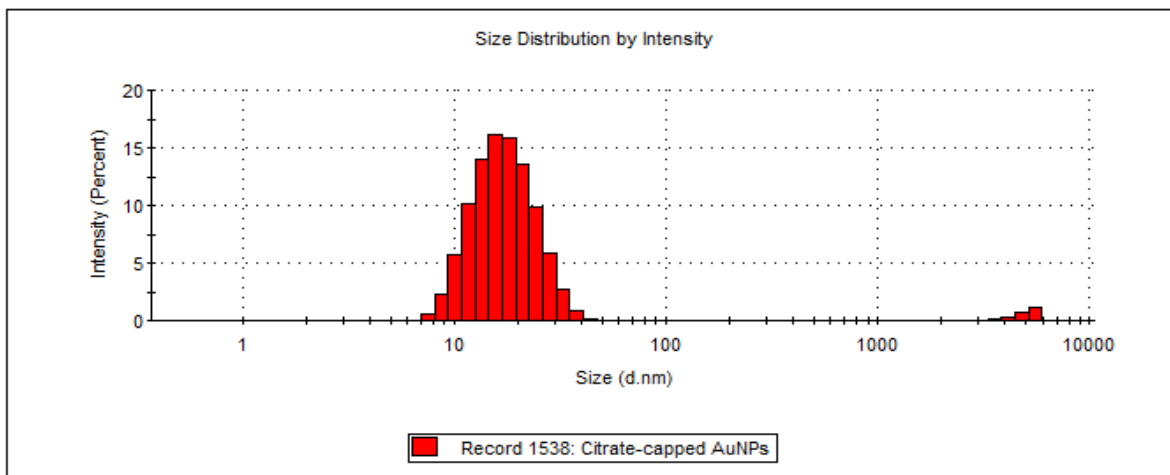


Figure 3.11: Size distribution of the citrate-capped AuNPs determined by the Malvern Zetasizer.

3.4.3 ζ -potential of the AuNPs

In this experiment, ζ - potential of the AuNPs was measured. The term ζ - potential describes the electrostatic potential around the particle surface. NPs bearing a ζ - potential between -10 mV and +10 mV are considered to be neutral, whereas NPs with a ζ - potential less than -30 mV or greater +30 mV are considered as charged and more likely remain stable in the solution. This is because they will not aggregate and will repel each other due to their electrostatic forces around the charges. On the other hand, the NPs with a ζ - potential greater than -30 mV or less than +30 mV are considered unstable and will eventually aggregate due to Van Der Walls inter-particle attraction (Nanocomposix, 2012).

The AuNPs showed a ζ - potential of -30.1 mV (**Figure 3.12**) which indicated that the AuNPs were highly stable and convenient for conjugation. The negative charge also indicated that the particle size was smaller than 100 nm, which was confirmed with the data obtained from UV-vis spectrophotometry and DLS. Other studies have reported synthesis of AuNPs with a ζ - potential of -43.2 mV (Lata *et al.*, 2015) and -44 mV (Nara *et al.*, 2010).

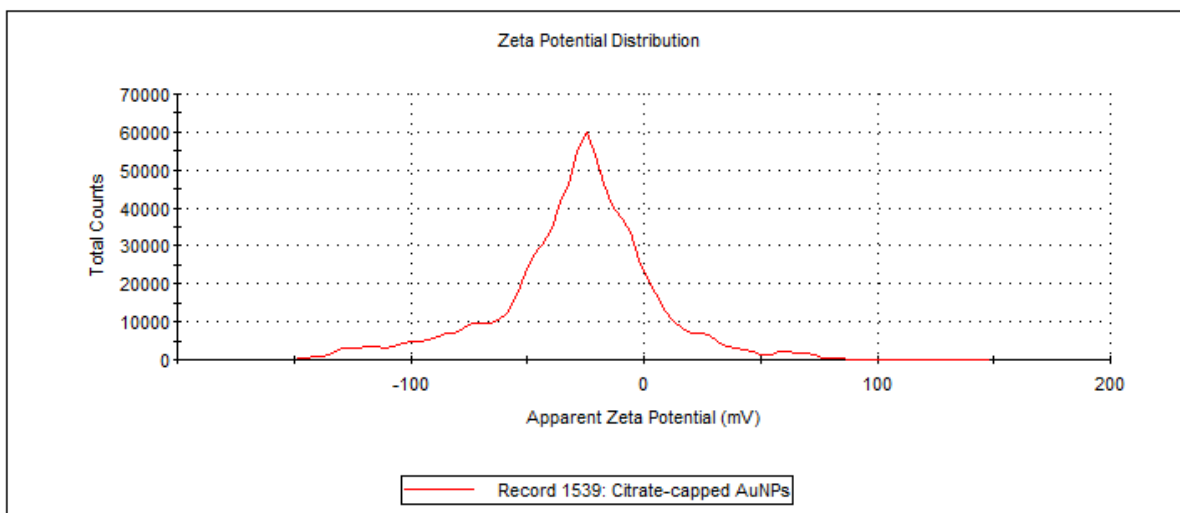


Figure 3.12: Zeta potential analysis of the citrate-capped AuNPs determined by the Malvern Zetasizer.

3.4.4 TEM analysis of the AuNPs

In order to confirm the results obtained, the AuNPs were further characterized by TEM. This technique is the most commonly used technique to determine the size, morphology, topography, composition and crystallography of the sample (Wang, 2001).

TEM images showed that the AuNPs were mostly spherical in shape (**Figure 3.13: A**). The images further revealed that the AuNPs were relatively monodispersed, this is due to the negatively charged layer of citrate ions which makes them to repel each other (Verma *et al.*, 2014). The AuNPs dispersion showed no sign of aggregation. The core diameters of AuNPs were found to be 13.59 ± 3.04 nm which corroborate the results obtained from the UV-vis spectrophotometry (**Figure 3.13 B**). This data corroborates other published results of citrate-capped AuNPs (cAuNPs) (Bai *et al.*, 2015; Verma *et al.*, 2014).

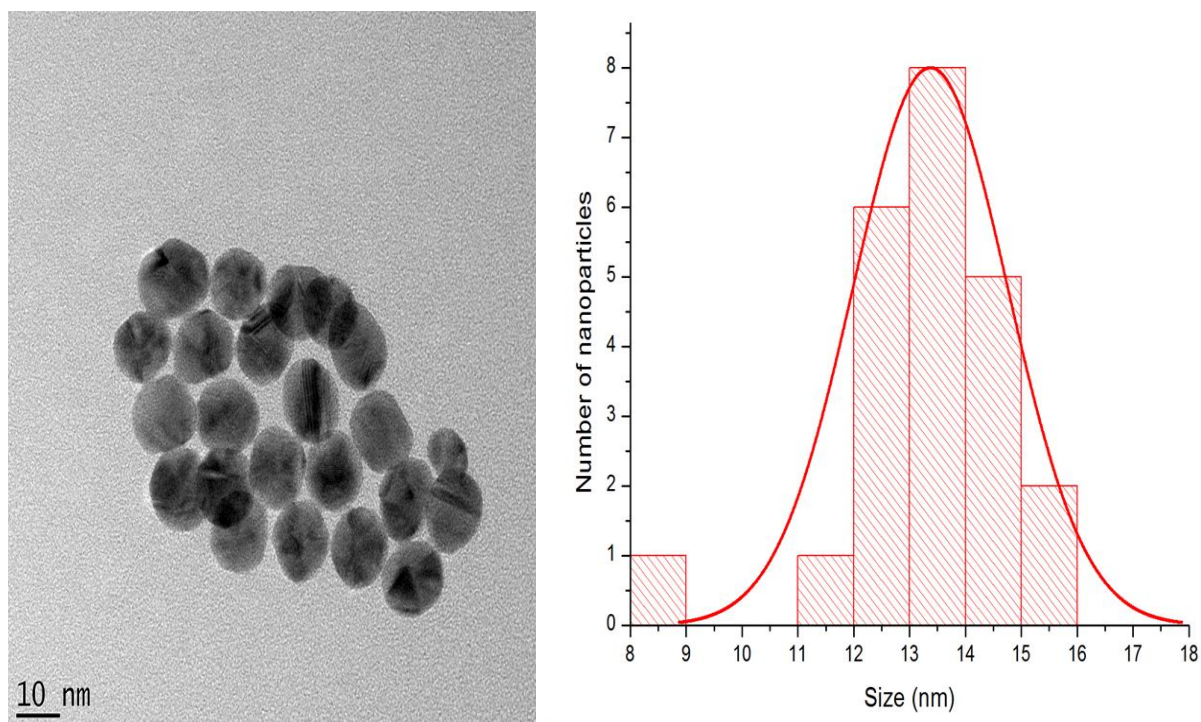


Figure 3.13: (A) TEM images of the citrate-capped AuNPs and (B) their size distribution. The magnification was at 10 nm. The core diameter of the AuNPs was calculated by measuring the circumference of 23 individual particles of the TEM images of AuNPs using the Image J software.

3.4.5 EDX analysis of the AuNPs

In order to validate the presence of Au in the NPs solutions, the energy dispersive x-ray spectra (EDX) of the AuNPs was carried. EDX is a technique used to obtain the elemental and chemical composition of NPs. It relies on the unique atomic structure of each element. Therefore, the x-ray spectrum emitted by different atomic structures is clearly distinct between different elements (Rao and Biswas, 2009).

The EDX spectrum of the AuNPs, in **Figure 3.14** shows the presence of gold (Au), which was expected. However, there are other traces of other elements such as copper (Cu), carbon (C) and oxygen (O). The presence of Cu and C was due to the holey carbon coated Ni/Cu grid that the AuNPs were placed on during the analysis whereas O may have been adsorbed onto the sample surfaces. The results are corroborated by Tejaswi *et al.* (2016) in which Au, Cu and O were also observed.

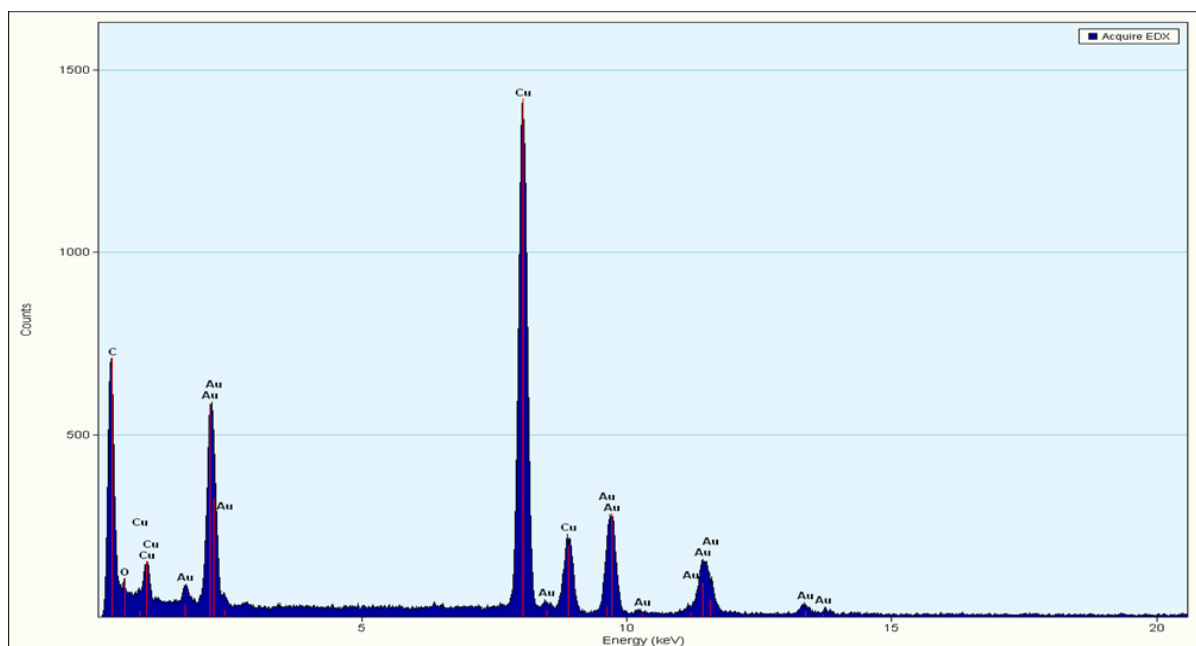


Figure 3.14: The chemical composition/EDX spectrum of the AuNPs.

3.5 Functionalization of ssDNA aptamer probe to AuNPs

3.5.1 Conjugation and characterization of apt-AuNP

The multifunctional properties of AuNPs offer unique opportunities for their use in the development of various diagnostic methods and devices. AuNPs prepared via citrate reduction method show uniformity, stability and wider applications in immunoassays (Thobhani *et al.*, 2010). Moreover, thiolated compounds (aptamers, antibodies, peptides) can adsorb onto the AuNPs due to the high affinity of gold for thiol; thus, enhancing their stability and functionality (Zhang *et al.*, 2012). Therefore, in this study, RBA-2 which was modified with thiol at its 5' end was used for conjugation to the AuNPs. To confirm that the thiolated aptamer probe conjugated to the AuNPs, samples were characterized using the UV-vis spectrophotometry, Zetasizer and Qubit assay. Stability tests were also done to detect any colour changes after conjugation.

3.5.1.1 UV-vis spectrometry of the apt-AuNPs

The UV-vis spectrophotometry has been widely used to determine the absorption spectrum of AuNPs in order to indicate immobilization of aptamers or other biomolecules on the surface of the AuNPs. AuNPs exhibit a strong λ_{\max} in the visible region that can be used to determine whether modification of the NP surface has been successful (Philip, 2008). The colloidal SPR depends on several factors such as the size, solvent and surface modification, and is useful in

distinguishing AuNPs conjugates as well as to monitor adsorption of the ssDNA aptamers on the surface of the AuNPs.

Figure 3.15 shows the UV-vis spectra of the AuNPs, and apt-AuNPs with and without NaCl. The red shift in optical properties of the apt-AuNPs conjugates indicated the adsorption of the aptamers on the surface of the AuNPs was successful. The λ_{\max} of AuNPs was obtained at 517 nm and shifted to 522 nm for 25 μM , 519 nm for 50 μM , 518 nm for 75 μM , and to 525 nm for 85 μM upon conjugation. The red shift could be attributed to successful conjugation of the aptamers to the AuNPs; whereas, a small decrease in the peak intensity of the AuNPs can be attributed to the decrease in the interparticles distance as a result of conjugation (Liu and Lu, 2006, Qadami *et al.*, 2018).



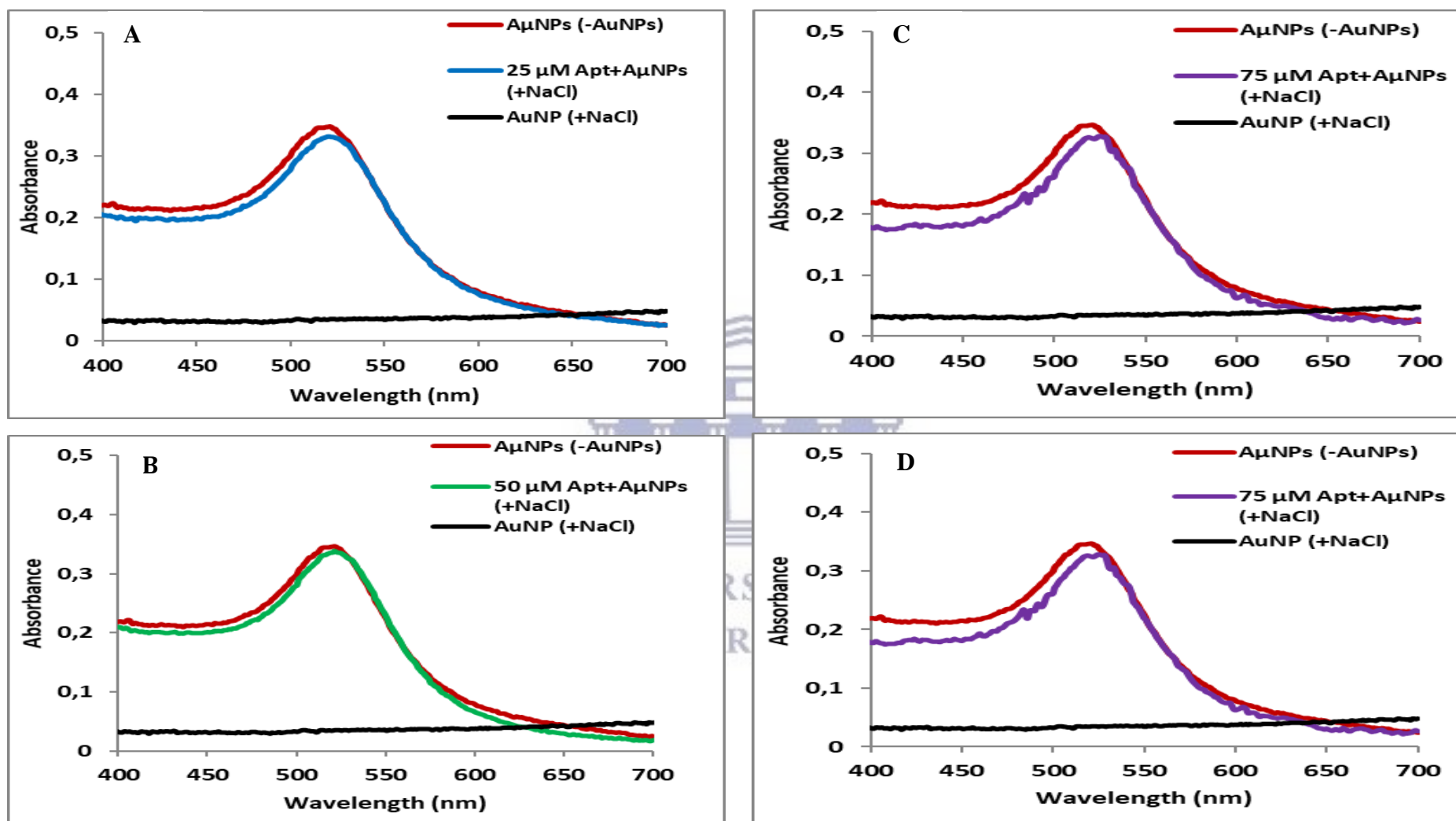


Figure 3.15: Comparison of the UV-Vis spectra of the AuNPs, apt-AuNPs conjugate with and without NaCl as indicated by +NaCl and -NaCl, respectively.

A: 25 μM aptamer concentration; B: 50 μM aptamer concentration; C: 75 μM aptamer concentration; D: 85 μM aptamer concentration.

3.5.1.2 Analysis of the stability of the apt-AuNPs conjugate

Visual detection, in which the changes in the colour of the AuNPs can be directly observed by the eyes, has gained a wide attention and serves as a preliminary characterization which does not require using any expensive and complicated instruments. It helps researchers to explore the stability of the AuNPs under various concentrations of proteins or aptamers. It is mostly applied in colorimetric assays in the presence of a target molecule (Guan *et al.*, 2014; Zhang *et al.*, 2012). Hence, this technique was used in this study to analyze the stability of the apt-AuNPs conjugates.

Figure 3.16, shows the obvious ruby-red to purple/blue colour change observed upon addition of NaCl in tube 1 (AuNPs). Addition of NaCl led to a slight colour change when 25 μM aptamer was used. This indicated that the surface of AuNPs was not fully covered by aptamers, hence the addition of NaCl caused aggregation (Ou *et al.*, 2010). In contrast, the colour of apt-AuNPs at 50 - 85 μM remained ruby-red which is the same colour as the AuNPs (tube 0). This indicated that the surface of the AuNPs was fully covered with aptamers via the thiol group. The absence of a color change at higher concentrations indicated that the apt-AuNPs were stable. Thus, the minimal aptamer concentration required to stabilize the AuNPs was 50 μM . The results are corroborated by the results obtained by Zhang *et al.* (2016) and Chen *et al.* (2015).



UNIVERSITY of the
WESTERN CAPE

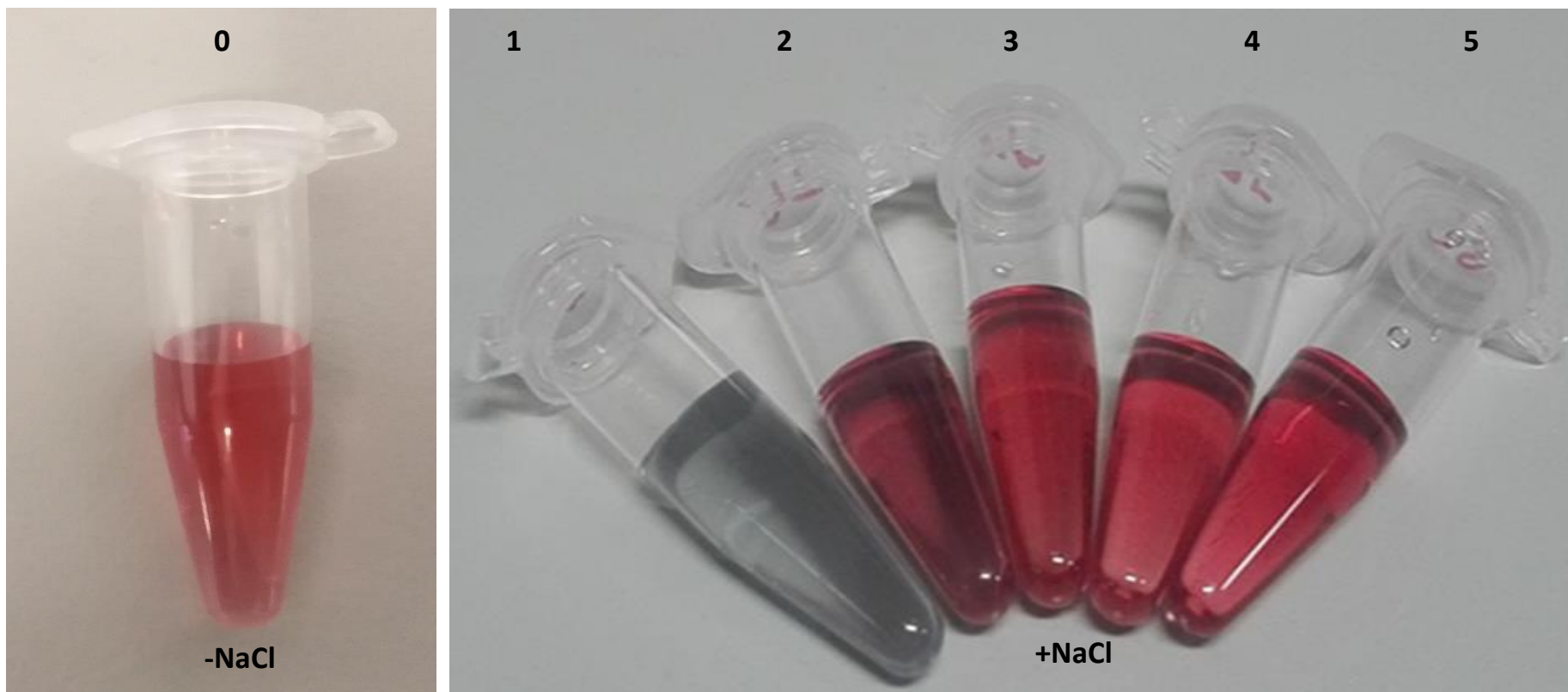


Figure 3.16: Colour change detection by naked eyes. Tube 0: AuNPs (-NaCl); Tube 1: 0 μM ; Tube 2: 25 μM ; Tube 3: 50 μM ; Tube 4: 75 μM ; Tube 5: 85 μM aptamer concentration and AuNPs (+NaCl).

3.5.1.3 DLS, PDI and ζ -potential analyses of the apt-AuNPs

DLS is able to monitor not only the core of NPs but also the surface modifications. Because adsorption of ssDNA probes onto AuNPs would cause an increase in the size of particles, DLS was used to evaluate adsorption by measuring sizes of the modified particles. It is well established that, at a low surface coverage, the ssDNA probe lays flat on the surface, due to non-specific binding. However, as the surface coverage increases, the aptamers start to adopt a more perpendicular conformation due to electrostatic repulsion between the aptamers and the AuNPs, which may lead to an increase in the hydrodynamic diameter (Liu and Liu, 2017).

In this experiment, the hydrodynamic diameter of the AuNPs was 16.82 and conjugation of aptamers to AuNPs had no significant effect on the hydrodynamic diameter, ~ 18 nm (17.85 - 18.42 nm) in the absence of NaCl. At 25 μ M aptamer concentration, the hydrodynamic diameter of the AuNPs increased to 54.66 nm; for 50 - 85 μ M, the hydrodynamic diameter increased upon the addition of salts to 31 nm (30.94 - 31.71 nm). The results further indicated that the optimal loading capacity of apt-AuNPs was at a concentration of 50 μ M.

The PDI results (**Table 3.3**) indicated that in the absence of NaCl, the AuNPs at all aptamer concentrations remained monodispersed. However, in the presence of NaCl, the PDI of the AuNPs at 0 and 25 μ M increased to 0.378 and 0.44, respectively. This indicated that the AuNPs were polydispersed; whereas, the results for higher concentrations (50 - 85 μ M) indicated that the AuNPs were still monodispersed with a PDI of 0.257 - 0.266. There were no major changes observed on the PDI (0.134 - 0.244) in the absence of NaCl.

Addition of aptamers had no effect on the ζ -potential of conjugated AuNPs compared to control (**Table 3.3**). The ζ -potential increased from -30.31 to -20.93 after exposing the apt-AuNPs to NaCl. These changes can be attributed to molecules attached to the AuNPs surfaces and could be used to predict how these AuNPs are going to behave when used in the LFA and also the shelf life of the LF.

Table 3.3: DLS, PDI and ζ -potential of the apt-AuNPs conjugate determined using the Zetasizer.

[Aptamer] (μM)	-NaCl			+NaCl		
	Z ave (nm)	PDI	Zeta pot.	Z ave (nm)	PDI	Zeta pot.
0	16.82	0.228	-30.31	658.2	0.378	-25.8
25	17.89	0.244	-35.2	54.66	0.44	-22.8
50	17.85	0.223	-28.9	30.94	0.266	-20.93
75	18.04	0.221	-34.8	31.71	0.265	-22.2
85	18.42	0.134	-29.6	31.70	0.257	-25.4

3.5.1.4 UV-vis spectrometry of the apt-AuNPs

The UV-vis spectrophotometry was used to check the absorption spectra after removing the unbound aptamers from the apt-AuNPs. The UV-vis spectra show (**Figure 3.17**) that the apt-AuNPs at 50 - 85 μM in the presence of NaCl were stable while apt-AuNPs in the absence of NaCl were not stable. Their SPR shifted to longer wavelength which resulted in a formation of a new peak between 600 - 700 nm, which indicated that there was aggregation (Zimbone *et al.*, 2014). This result was further corroborated by the visible colour change from ruby-red to dark purple/blue (shown by photograph insert).

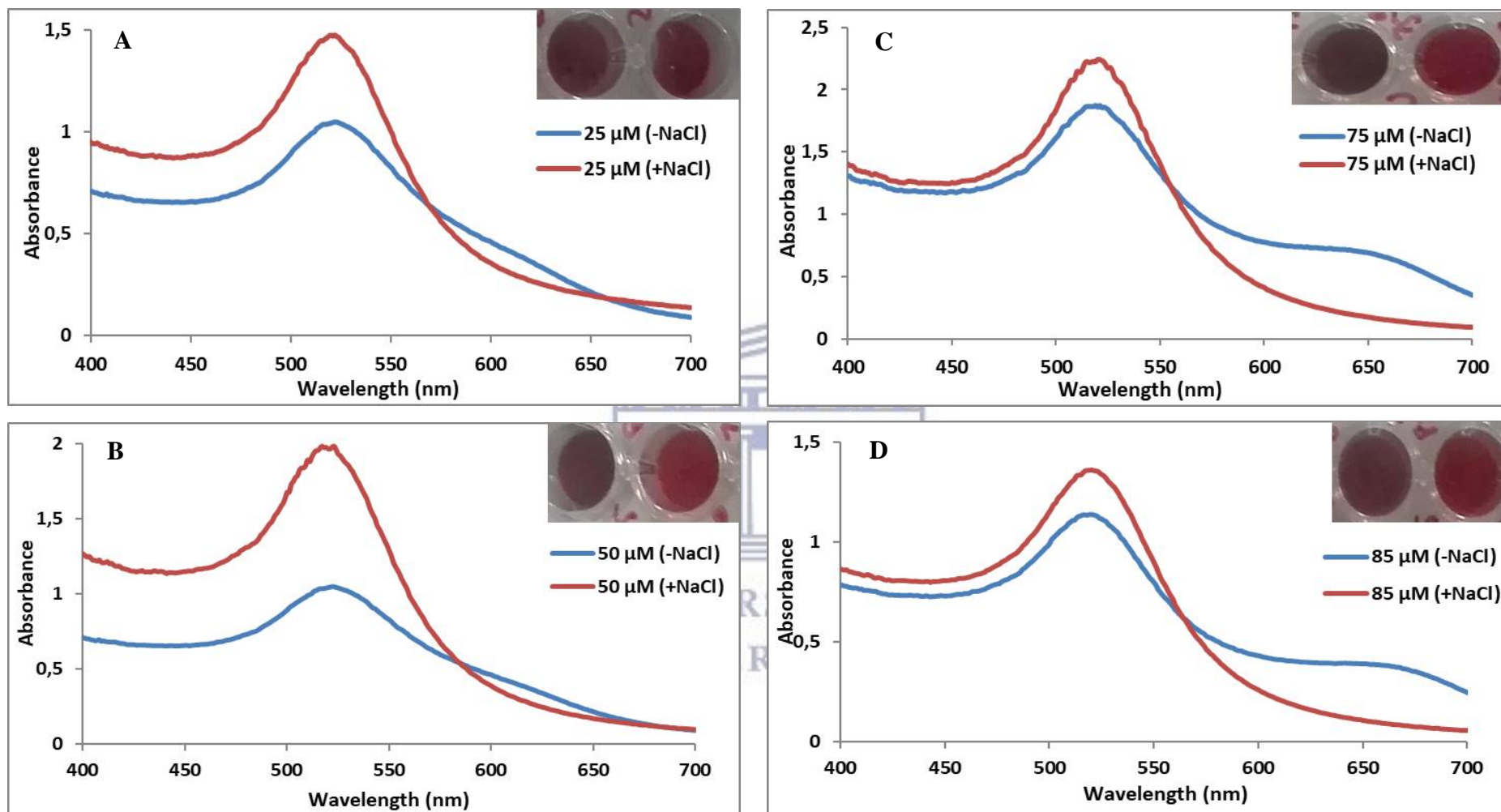


Figure 3.17: UV-vis spectra of the apt-AuNPs after removing the unbound aptamers. The maroon colour represent the apt-AuNPs in the presence of 1 M NaCl (+NaCl) and blue colour represent the apt-AuNPs in the absence of NaCl (-NaCl). A: 25 μM aptamer concentration; B: 50 μM aptamer concentration; C: 75 μM aptamer concentration; D: 85 μM aptamer concentration.

3.5.1.5 Quantification of ssDNA aptamer bound to AuNPs

To determine the concentration of the aptamers bound to the AuNPs, a reliable quantification of the ssDNA aptamer is important. The amount of the ssDNA aptamer after conjugation may be very low due to insufficient breaking of the disulphide bonds by TCEP, therefore, a sensitive assay for quantification is needed. The Qubit high-sensitivity assay which is able to accurately detect as little as 50 pg/ μ L of the sample was used for quantification. Besides its specificity, this assay is more advantageous than the Nanodrop as common contaminants such as salts, free nucleotides, solvents, detergent or protein that may be present in the sample are tolerated in the assay.

The results shown in **Table 3.4** indicated that a reliable quantification of 25 μ M was not possible. This could be attributed to the concentration not being sufficient to cover the whole surface of the AuNPs; thus, indicating that an increase in concentration is still needed. On the other hand, a reliable quantification of 14.6, 17.8 and 11.6 ng/mL were detected for 50, 75 and 85 μ M, respectively. Although the aptamer concentration in the conjugates was not directly quantified due to the quenching effect of AuNPs on the dye, the method used in this study support the results given by preliminary characterization and suggest that the aptamers at certain concentration were able to fully cover the surface of the AuNPs.

Table 3.4: Quantification of ssDNA by Qubit assay.

[Apt] (μ M)	[Apt in H ₂ O] (ng/mL)	[Unbound apt] (ng/mL)	[Bound apt] (ng/mL)
25	10.4	Samples too low	Not calculated
50	20.7	14.6	6.1
75	33.3	17.8	15.5
85	36.4	11.6	24.8

3.5.2 Conjugation and characterizations of RBA-2 to AuNPs (Large scale)

3.5.2.1 UV-vis spectrophotometry of the apt-AuNPs

Conjugation of the RBA-2 aptamer to AuNPs was done in a large scale for use in the development of the LF test strips. **Figure 3.18** shows the UV-vis spectra of the AuNPs, and apt-AuNPs conjugate. The λ_{\max} of AuNPs is obtained at 522 nm with a high symmetry and narrow width, which indicated that the prepared AuNPs were monodisperse and had narrow size distribution. The λ_{\max} of the AuNPs shifted to 525 nm upon conjugation with aptamers. The intensity of the apt-AuNPs conjugate peak was reduced compared with the unconjugated AuNPs peak. The red shift and the decrease in the peak intensity of the AuNPs may be attributed to the decrease in the interparticles distance as a result of apt-AuNPs conjugation (Aaryasomayajula *et al.*, 2014). However, the results were inconclusive because the presence of aptamers was not further confirmed by a peak at 260 nm because the AuNPs also showed a peak at 260 nm. Similar data was observed when the biotinylated RBA-2/15 mer' poly-T was used.

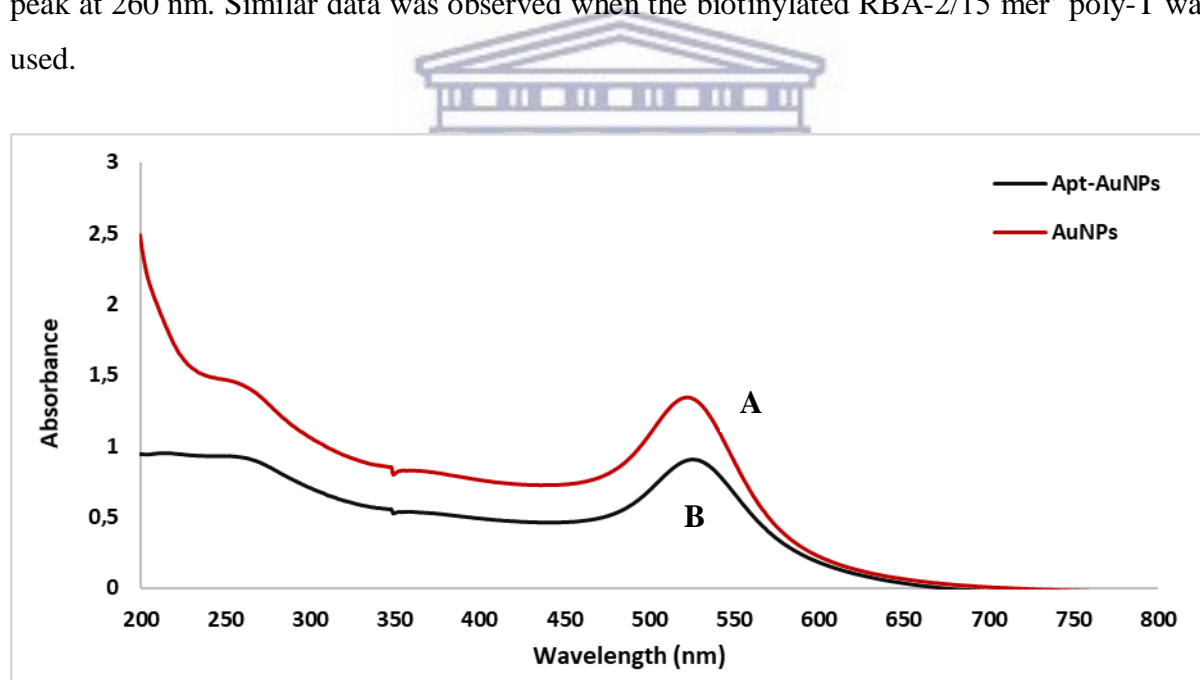


Figure 3. 18: UV-vis analysis of AuNPs and apt-AuNPs conjugates. (A) citrated-capped AuNPs; (B) 50 μ M of the biotinylated-RBA-2 was conjugated to the AuNPs.

3.5.2.2 Gel electrophoresis analysis of the apt-AuNPs

Gel electrophoresis was also used to confirm successful conjugation of the aptamer to the AuNPs based on the mobility shift effect. As indicated in **Figure 3.19**, in lane 2, the unconjugated AuNPs did not migrate into the gel and formed a black precipitate immediately after mixing with the loading dye. In lane 3, a distinct band, which corresponded with the apt-

AuNPs conjugates was observed. Lane 4 showed the aptamer band (arrow; at about 75 bp). The band was faint, which could be attributed to the low aptamer concentration used. There is a clear retardation in the apt-AuNPs migration along the gel (lane 3) compared to AuNPs alone. This can be attributed to both the increased size of the apt-AuNPs complex, as well as to each AuNPs bearing multiple copies of the aptamer. Furthermore, the colour of the AuNPs remained ruby-red, indicating that the AuNPs were still stable. Similar data was observed when the biotinylated RBA-2/15 mer' poly-T was used.

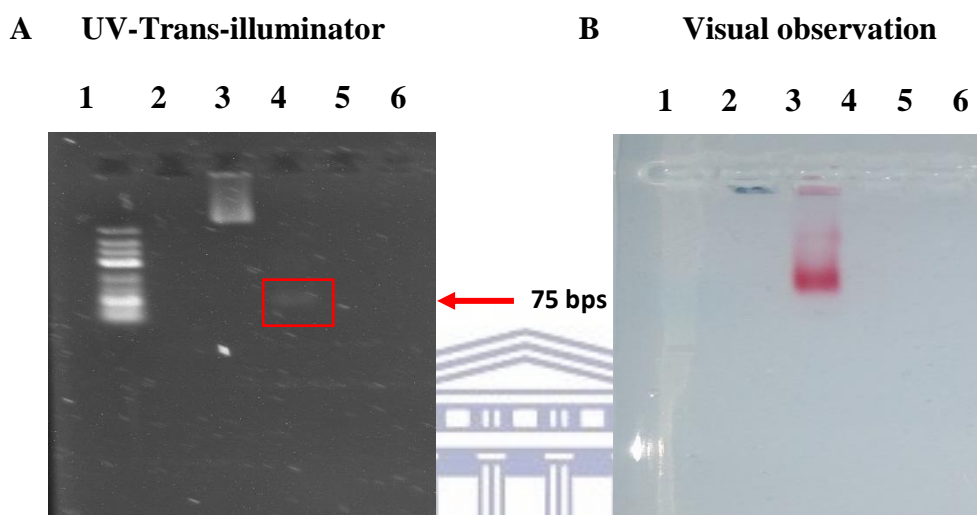


Figure 3.19: Analysis of apt-AuNPs conjugation by 1% agarose gel electrophoresis. Images were analyzed by (A) UVP Trans-illuminator and (B) visual observation. 1: 100 bp O' gene ruler; 2: AuNPs; 3: apt-AuNPs conjugate; 4: free aptamer (arrow).

3.6 Development of the lateral flow test strips

Previous studies have demonstrated the feasibility of developing strip biosensors based on aptamer-functionalized AuNPs for the detection of thrombin (Xu *et al.*, 2009), ochratoxin A (Zhou *et al.*, 2016) and vaspin (Raston *et al.*, 2017). For the extended application of RBP4 aptamers selected by Lee *et al.* (2008), we combined the high affinity, specificity, and stability of aptamers to develop an aptamer-based lateral flow test strips for rapid and sensitive detection of RBP4.

For the preparation of the test line on the lateral flow test strips, streptavidin was set as a bridge, which can be immobilized on the nitrocellulose membrane by electrostatic adsorption and linked biotin-modified aptamer through the specific reaction of streptavidin and biotin. This was done to prevent nucleic acid from being washed away easily by the sample flow when sprayed onto the nitrocellulose membrane directly because they have no specific

binding force to the nitrocellulose membrane. Then, RBP4 (0.5 mg/mL) prepared in PBS buffer was directly immobilized on the control line. When the apt-AuNPs conjugate mixture was wicked on the edge of the nitrocellulose membrane, it migrated through capillary action to interact with RBP4 on the control line.

Based on the results on **Figure 3.20**, there was an appearance of a line on the control line which was observed within five min. The presence of a line was regarded as positive results; however, the intensity of the line was weak and decreased gradually until it disappeared after washing with the 1× SELEX buffer which indicated that there is no interaction between the aptamer and the protein. It was postulated that the negative results obtained may be due to low concentration of the RBP4; thus, the concentration was increased to 2 mg/mL and the test strips were prepared in the similar manner as before. Nevertheless, the results were still negative. This could be attributed to the protein being subjected to desorption upon direct immobilization on the LF test strips. The presence of His-tag modification on the protein might also be a key factor that resulted to negative results.

Hence, a new experiment was performed with a new RBP4 protein (1.3 mg/mL) and thiolated RBA-2/15-mer poly-T. The use of spacers allows more space for the aptamers to fold into their active structure and therefore result in a higher ratio of functional aptamers. A biotin-modified poly-A aptamer was immobilized on the control. The choice of using the biotin-modified complementary poly-A aptamer was because the new set of aptamer incorporated a 15 mer' poly-T spacer.

The results obtained in **Figure 3.21** indicated that before wash, there was a band obtained at the test line and the unbound labelled reporter aptamer conjugate migrated along the nitrocellulose membrane and was captured at the control line by the biotinylated poly-A aptamer; whereas, other excessive solutions went to the absorption pad. The intensity of the colour at the control line corresponds to the amount of the unbound aptamer captured by the complementary aptamer. The band, which was initially obtained at the test line, had a weak intensity and gradually disappeared after washing with 1× SELEX buffer.

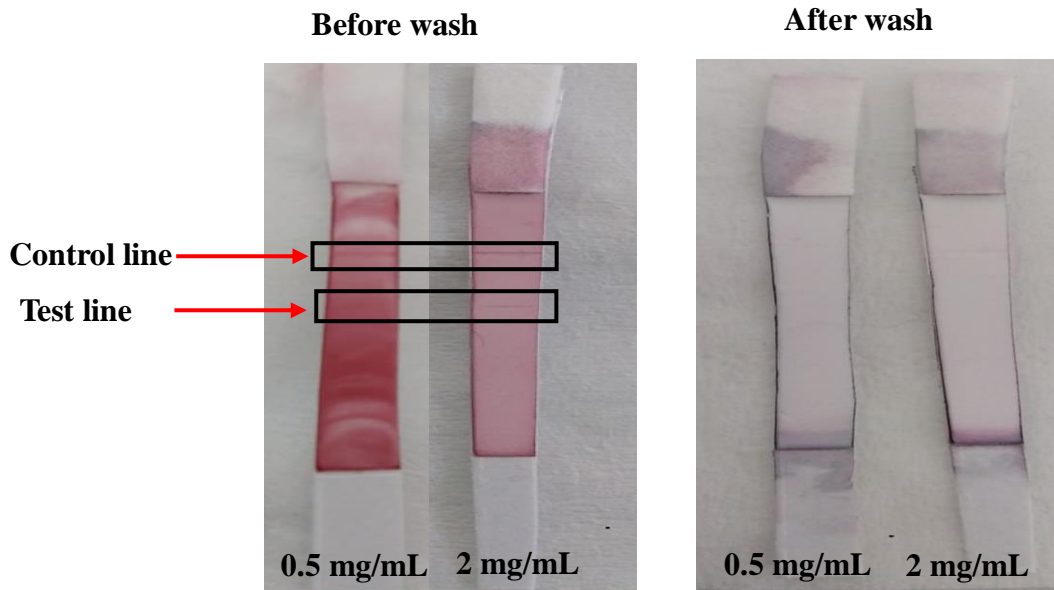


Figure 3.20: Detection of RBP4 (0.3 - 2 mg/mL) by the conventional LFA. RBP4 was immobilized on the control line and RBA-1 was immobilized on the test line.

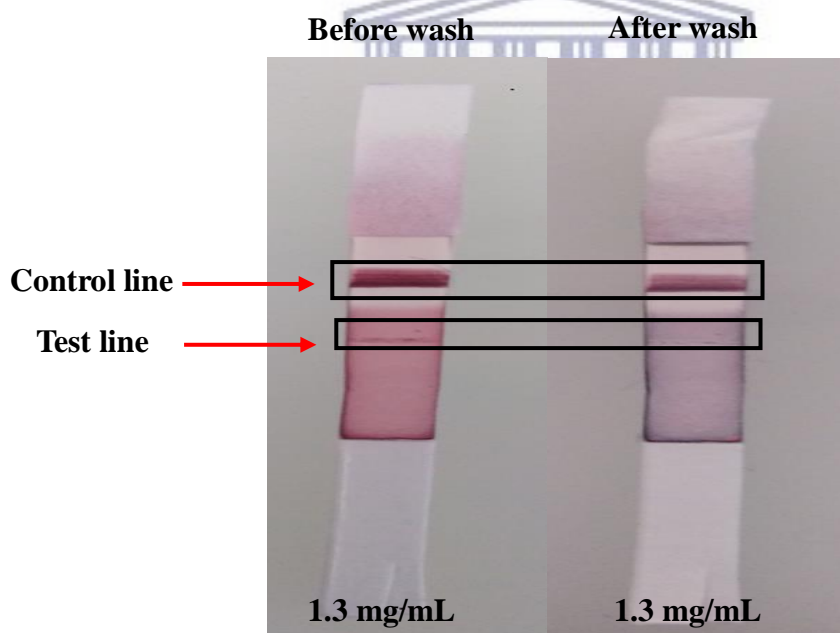


Figure 3.21: Detection of RBP4 (1.3 mg/mL) by the conventional LFA. RBP4 was immobilized on the test line and biotinylated poly-A aptamer was immobilized on the control line.

3.7 Development of a colorimetric aptasensor

The present study further investigated the possibility of developing a colorimetric aptasensor for the detection of RBP4. This assay is based on colour change from ruby-red to blue/purple due to conformational change of aptamer in the presence of the target molecule, and the phenomenon of salt-induced AuNPs aggregation which could be monitored by eyes or UV-vis spectrophotometer.

3.7.1 Determination of the optimum concentration of NaCl and aptamer

It is well known that AuNPs are highly reactive and aggregate easily in the presence of salts, so it is important to monitor the salt-induced AuNPs aggregation kinetics for the development of a colorimetric aptasensor. To optimize the performance of the developed assay, various conditions such as, RBA-2/15 mer' poly-T and NaCl concentrations were investigated, as described in **Section 2.2.6.1**.

Figure 3.22 indicate the photograph insert of the reaction conditions (**A**) and the absorbance ratio (A_{660}/A_{520}) (**B**). It was apparent that the AuNPs with and without aptamers barely aggregated under 20 mM NaCl solution. The control AuNPs (without the aptamer) changed colour from ruby-red to purple/blue with an increased NaCl concentration (40 - 100 mM) and the percentage aggregation kinetics increased and reached saturation at 80 and 100 nM. Thus, the minimum required NaCl is 60 nM. The observation suggested that the Na^+ and Cl^- ions destroyed the ionic environment and led to the aggregation of AuNPs in the absence of aptamers. Addition of 25 nM aptamer, partially protected the AuNPs; whereas, it can be seen that when the aptamer concentration were 50 - 100 nM, the protection efficiency against salt-aggregation of AuNPs was excellent which was indicated by the ruby-red colour and a lower percentage aggregation kinetics.

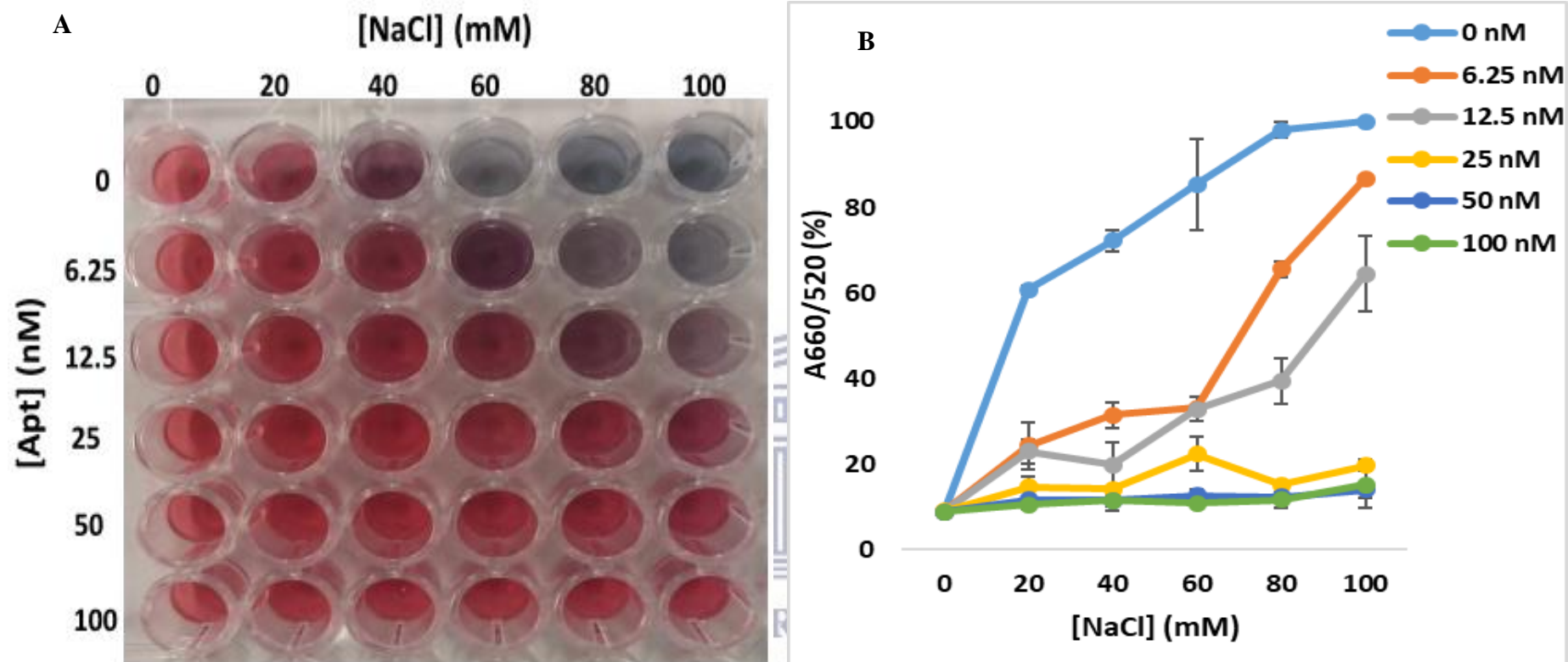
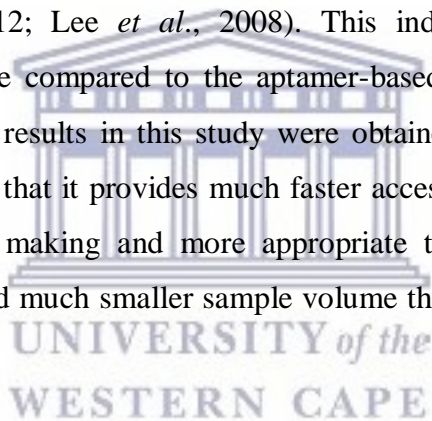


Figure 3.22: Optimization of the biotinylated-aptamer and NaCl concentrations for the development of the aptasensor. (A) Photograph insert; (B) Absorbance ratio. Final aptamer concentrations: 0, 6.25, 12.5, 25, 50 and 100 nM; final NaCl concentrations: 0, 20, 40, 60, 80 and 100 mM.

3.7.2 Sensitivity of the aptasensor for RBP4 detection

The sensitivity of the colorimetric sensor for the detection of RBP4, under the optimized experimental conditions, was measured with different concentrations of RBP4 as described in **Section 2.2.6.2**.

Figure 3.23 shows that the colour of the AuNPs changed from ruby-red to purple/blue (insert) and the absorbance ratio (A_{600}/A_{520}) gradually increased with an increase of RBP4 concentration. The results demonstrate that RBA-2 bound to RBP4; thus, detached from the AuNPs, leaving the AuNPs unprotected. In the presence of 60 mM NaCl, the AuNPs aggregated. The aggregation was confirmed by the red shift from 520 nm to 600 nm as indicated by **Figure 3.23: A**. The assay was reproducibly sensitive with a limit of detection of 45.32 nM ($R^2 = 0.9656$) (**Figure 3.23: B**). The detection limits of the same protein obtained using ELAA and aptamer-based SPR analysis were 0.45 and 75 nM (**Table 3.5**), respectively (Lee *et al.*, 2012; Lee *et al.*, 2008). This indicated that the colorimetric aptasensor was more sensitive compared to the aptamer-based SPR; but, less sensitive as compared to the ELAA. The results in this study were obtained within 5 min. One of the major advantages of POCT is that it provides much faster access to test results, allowing for more rapid clinical decision making and more appropriate treatments and interventions. Moreover, the method required much smaller sample volume than those needed for testing in the central clinical laboratory.



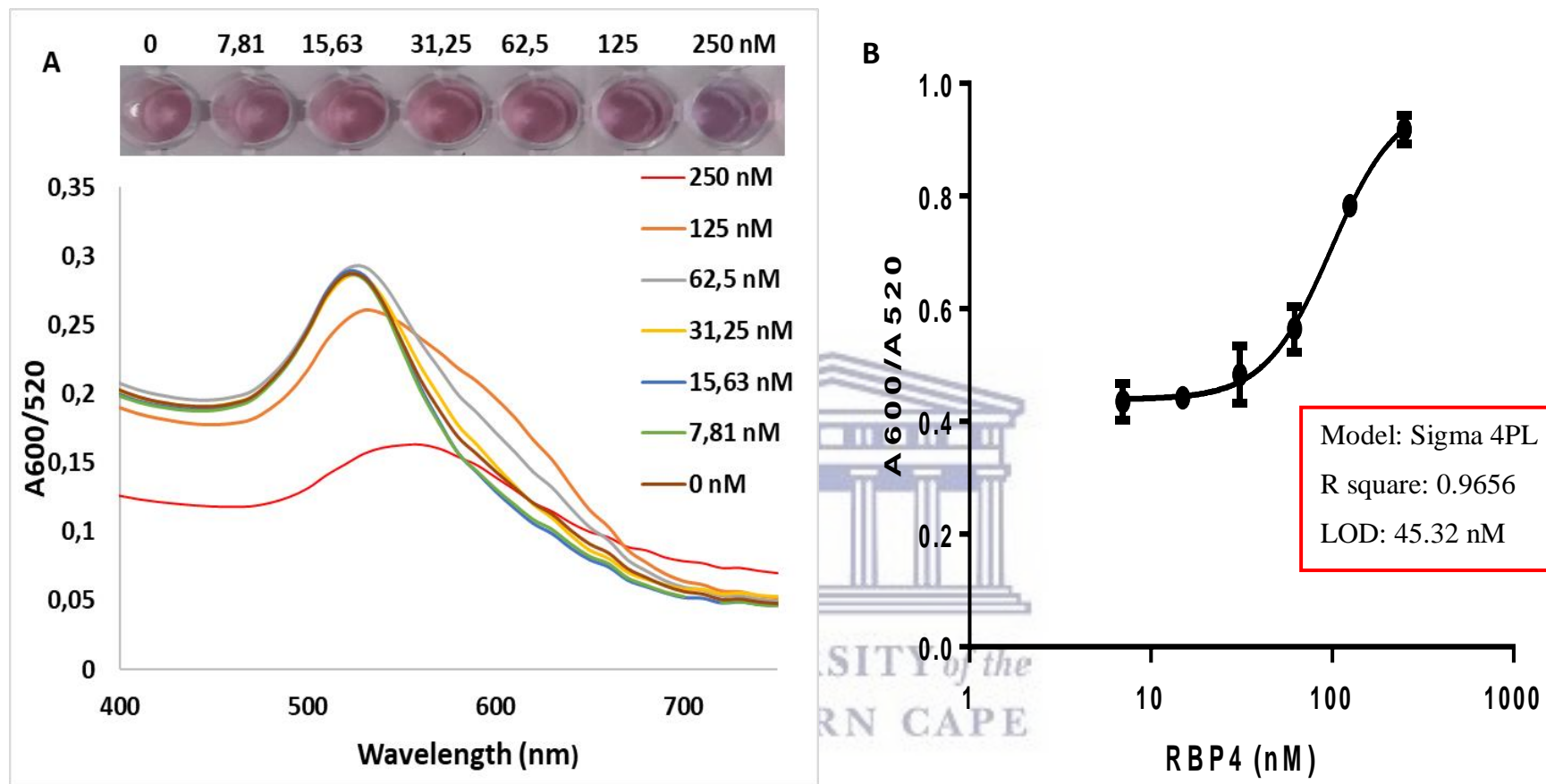


Figure 3.23: Sensitivity analysis of the colorimetric aptasensor. A: Absorption spectra of apt-AuNPs solutions treated with different RBP4 concentrations. Inset: visual colour changes of the sensing solution treated with 0, 7.81, 15.63, 31.25, 62.5, 125, 250 nM RBP4. B: Standard curve for different absorbance intensity (A_{600}/A_{520}) corresponding to different concentrations of RBP4. Each data point represents the averaged results of four separate experiments, each with two replicates.

Table 3. 5: Comparison of the colorimetric aptasensor with other methods for RBP4 detection.

Materials	Method	Limit of detection (nM)	Ref.
AuNPs and aptamer	Colorimetric	45.32	Present study
Aptamer and antibodies	ELAA	0.46	Lee <i>et al.</i> (2012)
Aptamer	SPR	75	Lee <i>et al.</i> (2008)



UNIVERSITY *of the*
WESTERN CAPE

CHAPTER 4: CONCLUSION

4.1 Conclusion

The aim of the present study was to characterize RBP4 aptamers for the development of aptamer-based PoC diagnostic kit for diabetes. The aptamer were previously selected by Lee *et al.* (2008) and the sequences were analysed using bioinformatics tools in order to determine their secondary structures. The interactions of these aptamers with RBP4 was evaluated by SPR (**Section 3.2**). The secondary structures correlated with the findings of kinetic studies which revealed high binding affinities of aptamers to RBP4 and enhanced stability as denoted by the stem hairpin loops. Binding of the aptamers to RBP4 was in a low nM range for three aptamers and pM for one aptamers, which is the preferred range that allows binding in seconds to minutes only (Svobodová, *et al.*, 2012). The results were further validated by ELAA and EMSA; however, the EMSA results were inconclusive. Even though ELAA showed binding of the aptamers to RBP4, there should be more optimization steps for improving the results. Sandwich-SPR demonstrated that RBA-1 and RBA-2 bind to different sites on RBP4 and the results were validated by sandwich-ELAA.

AuNPs were successfully synthesized and characterized. The AuNPs had an average size of 14 nm and λ_{\max} of 517 nm; a PDI of 0.226 and ζ - potential of -30.31 mV. The latter indicated that the AuNPs were indeed stable. TEM analysis revealed that the AuNPs were monodispersed and spherical. All the characterizations indicate that AuNPs are negatively charged, stable and convenient for the functionalization with aptamers. Conjugation of the aptamers to the AuNPs was achieved and used for the development of lateral flow test strips.

The development of the LF test strips was unsuccessful. Only one test strip showed positive results; however, the intensity was low and the results were not reproducible when different apt-AuNPs dilutions and also high concentrations of the RBP4 were used. Although, the LF test strips gave negative results, the present study has demonstrated the feasibility of developing an aptamer-based LFA for the detection of T2DM biomarker. Thus, further optimizations of different types of membranes, buffers, pH and target concentrations, are needed in order to obtain better resolutions and intensity on the test strips. The present study has successfully developed label-free aptasensor assay for RBP4 detection with a detection limit of 45.32 nM. The principle of such high sensitivity for RBP4 detection was based on the aggregation of AuNPs controlled by the salt induced and the special interactions between

RBA-2 and RBP4. The results indicated that the developed method had a relatively stable precision and satisfactory reproducibility. Therefore, the study has shown successful development of a simple yet effective colorimetric assay for RBP4 detection and the assay is not limited to this target, but also other targets with aptamers available without any special laborious instruments.

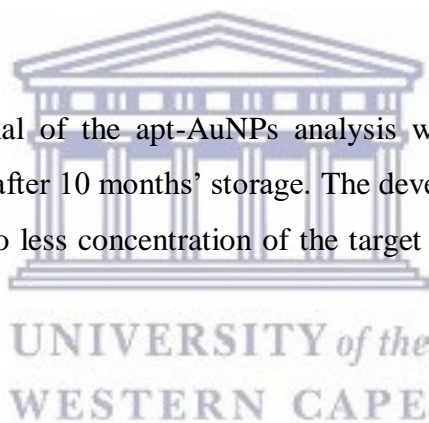
4.2 Limitation of the study

The present study has limitations that need to be addressed. The obtained sensorgrams showed specific shift at the beginning of association phase in majority of curves which complicated the fitting. The ELAA results for the identification of dual aptamers were not reproducible. The limitation factor was the newly ordered protein. Furthermore, the results obtained by EMSA analysis does not provide conclusive evidence of interaction, which may be due to the aptamers binding near the His-tag modification and or the incorrect gel percentage used.

The size, PDI and ζ - potential of the apt-AuNPs analysis was not repeated because the AuNPs were no longer stable after 10 months' storage. The development of LF test strips was not successful; perhaps, due to less concentration of the target protein, incorrect buffers and pH used.

4.3. Future studies

Future studies will include aptamer characterizations using different techniques such as a BLI and MST to validate the binding affinities of the aptamers and to identify dual aptamers. Different parameters such as different membranes, buffers, and target concentration will be optimized for the development of LF test strips. The stability of the AuNPs over a certain period will also be monitored in order to provide an insight on the shelf life of the LF test strips to be designed.



REFERENCES

- Aaryasomayajula, V.S.R., Severs, T., Ghosh, K., DeLong, R., Zhang, X., Talapatra, S. and Wanekaya, A.K. (2014). Assembly of a Dual Aptamer Gold Nanoparticle Conjugate Ensemble in the Specific Detection of Thrombin when Coupled with Dynamic Light Scattering Spectroscopy *Journal of Nanomedicine and Nanotechnology*, **5**(4): 1–6.
- Abel, E.D., Peroni, O., Kim, J.K., Kim, Y.B., Boss, O., Hadro, E., Minnemann, T., Shulman, G.I. and Kahn, B.B. (2001). Adipose-selective targeting of the GLUT4 gene impairs insulin action in muscle and liver. *Nature*, **409**: 729–733.
- Adhikar, M., Strych, U., Kim, J., Goux, H., Dhamane, S., Poongavanam, M.V., Hagstrom, A.E.V., Kourentzi, K., Conrad, J.C. and Willson, R.C. (2015). Aptamer-phage reporters for ultrasensitive lateral flow assays. *Analytical Chemistry*, **87**: 11660-11665.
- Agnihotril, N.P. and Bhide, M. (2012). Design of Aptamer-Gold Nanoparticles Based Colometric Assay for the Early diagnosis of Breast Tumour. *International Journal of Science and Research*, **3**(11): 2319–7064.
- Al-Tarawneh, S.K., Border, M.B., Dibble, C.F., Bencharit, S. (2011). Defining salivary biomarkers using mass spectrometry-based proteomics: a systematic review. *OMICS*, **15**: 353 – 361.
- Al-Tarawneh, S.K., Bencharit, S. (2009). Applications of Surface-Enhanced Laser Desorption/Ionization Time-Of-Flight (SELDI-TOF) mass spectrometry in defining salivary proteomic profiles. *Open Dentistry Journal*, **3**: 74–79.
- Almasi, F., Mousavi Gargari, S.L., Bitaraf, F. and Rasoulinejad, S. (2016). Development of a single stranded DNA aptamer as a molecular probe for Incap cells using cell-selex. *Avicenna Journal of Medical Biotechnology*, **8**: 104–111.
- Alsager, O.M., Alotaibi, K.M., Alswieleh, A.M., and Alyamani, B.J. (2018). Colorimetric Aptasensor of Vitamin D3: A Novel Approach to Eliminate Residual Adhesion between Aptamers and Gold Nanoparticles. *Scientific reports*, **8**: e12947.

American Diabetes Association, (2018). Classification and Diagnosis of Diabetes: Standards of Medical Care in Diabetes. *Diabetes Care*, **41**(1): S13–S27.

American Diabetes Association, (2014). Diagnosis and classification of diabetes mellitus. *Diabetes Care*, **37**(11): 8S1–S90.

American Diabetes Association. (2011). Standards of medical care in diabetes—2011. *Diabetes Care*, **34**(1): S11–S61.

American Diabetes Association (ADA). (2009). Diagnosis and Classification of Diabetes Mellitus. *Diabetes Care*, **40**(11): S9.

Amendola, V. and Meneghetti, V. (2009). Size evaluation of gold nanoparticles by UV - vis spectroscopy. *Journal of Physical Chemistry C*, **113**(11): 4277–4285.

American Diabetes, Association (2007). "Diagnosis and classification of diabetes mellitus". *Diabetes Care*. **30**(1): 42–47.

Aravindhaha Babu N., Masthan, N.K.M.K., Tathagat Bhattacharjee, T. and Elumali, M. (2014). Saliva the key regulator of oral changes in diabetes patients. *International Journal of Pharmaceuticals Science and Reseach*, **5**(7): 2579–2583.

Arguedas, J.A, Leiva, V. and Wright, J.M. (2013). Blood pressure targets for hypertension in people with diabetes mellitus. *The Cochrane Database of Systematic Reviews*, **10**: CD008277.

Aring, A.M., Jones, D.V., Falko, J.M. (2005). Evaluation and prevention of Diabetic Neuropathy. *American Family Physician*, **71**: 2123–2128.

Assadollahi, S., Reiningger, C., Palkovits, R., Pointl, P. and Schalkhammer, T. (2009). From lateral flow devices to a novel nano-color microfluidic assay. *Sensors (Basel, Switzerland)*, **9**(8): 6084– 6100.

Backus, K.M., Correia, B.E., Lum, K.M., Forli, S., Horning, B.D., González-Páez, G.E., Chatterjee, S., Lanning, B.R., Teijaro, J.R., Olson, A.J., Wolan, D.W, and Cravatt B.F.

(2016). Proteome-wide covalent ligand discovery in native biological systems. *Nature*, **534**(7608): 570–574.

Bai, W., Zhu, C., Liu, J., Yan, M., Yang, S. and Chen, A. (2015). Gold nanoparticle–based colorimetric aptasensor for rapid detection of six organophosphorous pesticides. *Environmental Toxicology and Chemistry*, **34**(10): 2244–2249.

Berg, K., Lange, T., Mittelberger, F., Schumacher, U. and Hahn, U. (2016). Selection and Characterization of an $\alpha 6\beta 4$ Integrin blocking DNA Aptamer. *Molecular Therapy-Nucleic Acids*, **5**: e294.

Berlanga-Acosta, J., López-Saura, P., Guillen-Pérez, I., Guillen-Nieto, G., Acevedo-Castro B, and Herrera- Martínez, L. (2013). Type 2 Diabetes Mellitus (T2DM): Biological Overview from Pathways to Organelles and its Translation toward a Torpid Wound Healing Process. *Journal of diabetes and metabolism*, **4**: e285.

Bertram, M.Y., Jaswal, A.V., Van Wyk, V.P., Levitt, N.S. and Hofman, K.J. (2013). The non-fatal disease burden caused by type 2 diabetes in South Africa, 2009. *Global Health Action*, **6**: e19244.

Bhalla, N., Jolly, P., Formisano, N. and Estrela, P. (2016). Introduction to biosensors. *Essays in Biochemistry*, **60**(1): 1–8.

Bian, C., Zhang, F., Wang, F., Ling, Z., Luo, M., Wu, H., Sun, Y., Li, J., Li, B., Zhu, J., Tang, L., Zhou, Y., Shi, Q., Ji, Y., Tian, L., Lin, G., Fan, Y., Wang, N. and Sun, B. (2010). Development of retinol-binding protein 4 immunocolloidal gold fast test strip using high-sensitivity monoclonal antibodies generated by DNA immunization. *Acta Biochim Biophys Sin*, **42**: 847–853.

Blind, M. and Blank, M. (2015). Aptamer selection technology and recent advances. *Molecular Therapy-Nucleic Acids*, **4**(1): e223.

Borth, W. (1992). Alpha 2-macroglobulin, a multifunctional binding protein with targeting characteristics. *The FASEB Journal*, **6**(15): 3345–3353.

Brereton, M.F., Rohm, M., Shimomura, K., Holland, C., Tornovsky-Babeay, S., Dadon, D., Iberl, M., Chibalina, M.V., Lee, S., Glaser, B., Dor, Y., Rorsman, P., Clark, A. and Ashcroft, F.M. (2016). Hyperglycaemia induces metabolic dysfunction and glycogen accumulation in pancreatic β -cells. *Nature Communications*, **(7)**: e13496.

Cabrera Escobar MA, Veerman JL, Tollman SM, Bertram MY, Hofman KJ (2013) Evidence that a tax on sugar sweetened beverages reduces the obesity rate: a meta-analysis. *BMC Public Health*, **13**: e1072.

Campfield, L.A, Smith, F.J., and Burn, P. (1996). The OB protein (leptin) pathway—a link between adipose tissue mass and central neural networks. *Hormone and Metabolic Research*, **28**(12): 619–632.

Carvalho, R.F., Kfoury, M.S., Piezzate, M.H., Gobbi, A.L. and Kubota, L.T. (2010). Electrochemical detection in a paper-based separation device. *Analytical Chemistry*, **82**(3): 1162–1165.

Cella, L.N., Sanchez, P., Zhong, W., Myung, N. V., Chen, W., and Mulchandani, A. (2010). Nano Aptasensor for Protective Antigen Toxin of Anthrax. *Analytical Chemistry*, **82**(5): 2042–2047.

Chang, A.L., McKeague, M., Liang J.C. and Smolke C.D. (2014). Kinetic and Equilibrium Binding Characterization of Aptamers to Small Molecules using a Label-Free, Sensitive, and Scalable Platform. *Analytical Chemistry*, **86**: 3273–3278.

Chen, D., Zhang, C., Lin, J., Song, X. and Wang, H. (2018.) Screening differential circular RNA expression profiles reveal that hsa_circ_0128298 is a biomarker in the diagnosis and prognosis of hepatocellular carcinoma. *Cancer Management and Research*, **10**: 1275–1283.

Chen, A. and Yang, S. (2015). Replacing antibodies with aptamers in lateral flow immunoassay. *Biosensors and Bioelectronics*, **71**: 230–242.

Chen, C., Luo, M., Ye, T., Li, N., Ji, X. and He, Z. (2015). Sensitive colorimetric detection of protein by gold nanoparticles and rolling circle amplification. *Analyst*, **140**: 4515–4520

- Chen, F., Zhou, J., Luo, F.L., Mohammed, A.B. and Zhang, X.L. (2007). Aptamer from whole-bacterium SELEX as new therapeutic reagent against virulent Mycobacterium tuberculosis. *Biochemical and Biophysical Research Communications*, **357**: 743–748.
- Chovelon, B., Durand, G., Dausse, E., Toulmé, J., Faure, P., Peyrin, E. and Ravelet, C. (2016). ELAKCA: Enzyme-Linked Aptamer Kissing Complex Assay as a Small Molecule Sensing Platform. *Analytical Chemistry*, **88**(5): 2570–2575.
- Chung, T., Hsu, K., Chen, J., Liu, J., Chang, H., Li, P., Huang, C., Shieh, Y. and Lee, C. (2016). Association of salivary alpha 2-macroglobulin levels and clinical characteristics in type 2 diabetes. *Journal of Diabetes Investigation*, **7**(2): 190–196.
- Comucci, E.B., Vasques, A.C., Geloneze, B., Calixto A.R., Pareja J.C. and Tambascia, M.A. (2014). Serum levels of retinol binding protein 4 in women with different levels of adiposity and glucose tolerance. *Brazilian Society of Endocrinology and Metabolism*, **58**(7):709–714.
- Coppari R (2017). Diabetes present and future. *The International Journal of Biochemistry and Cell Biology*, **88**: e197.
- Cordera, R. and Adami, G.F. (2016). From bariatric to metabolic surgery: Looking for a "disease modifier" surgery for type 2 diabetes. *World Journal of Diabetes*, **7**(2): 27–33.
- Covantev, S., Chiriac, A., Perciuleac, L. and Zozina, V. (2016). Maturity onset diabetes of the young: Diagnosis and treatment options. *Russian Open Medical Journal*, **5**(4): e402
- Daniels, D.A., Chen, H., Hicke, B.J., Swiderek, K.M. and Gold, L. (2003). A tenascin-c aptamer identified by tumor cell selex: Systematic evolution of ligands by exponential enrichment. *Proceedings of the National. Academy of Science USA*, **100**: 15416–15421.
- Darmostuk, M., Rimpelova, S., Gbelcova, H. and Ruml, T. (2015). Current approaches in SELEX: An update to aptamer selection technology. *Biotechnology Advances*, **33**: 1141–1161.
- Deshpande, A.J., Harris-Hayes, M. and Schootman, M. (2008). Epidemiology of diabetes and diabetes related complications. *Physical Therapy*, **88** (11): 1254–1264.

Dhiman, A., Kalraa, P, Bansal, V., Bruno J.G. and Sharma T.K. (2017) Review: Aptamer-based point-of-care diagnostic platforms. *Sensors and Actuators B: Chemical*, **246**: 535–553.

DiMatteo, M.R., Giordani, P.J., Lepper, H.S. and Croghan, T.W. (2002). Patient adherence and medical treatment outcomes: A meta-analysis. *Medical Care*, **40**(9):794–811.

Dinneen, S.F. (2006). What is diabetes? *MPMED Medicine*, **34**(2): 45-46.

Dizgah, I.M. (2013). Stimulated saliva glucose as a diagnostic specimen for detection of diabetes mellitus. *Journal of Archives in Military Medicine*, **1**(1): 24–27.

Drescher, D.G., Ramakrishnan, N.A. and Drescher M.J. (2009). Surface Plasmon Resonance (SPR) Analysis of Binding Interactions of Proteins in Inner-Ear Sensory Epithelia. *Methods in Molecular Biology*, **493**: 323–343.

Duan, N., Gong, W., Wu, S. and Wang, Z. (2017). An ssDNA library immobilized SELEX technique for the selection of an aptamer against Ractopamine. *Analytica Chimica Acta*, **961**: 100–105.

Duan, N., Ding, X.Y., Wu, S.J., Xia, Y., Ma, X.Y., Wang, Z.P. and Chen, J. (2013). In vitro selection of a DNA aptamer targeted against *Shigella dysenteriae*. *Journal of Microbiological. Methods*, **94**: 170–174.

Dunmore, S.J. and Brown, J.E. (2013). The role of adipokines in beta cell failure of type 2 diabetes. *Journal of Endocrinology*, **216**(1): 37–45.

Eaton BE, Gold L and Zichi DA (1995). Let's get specific: the relationship between specificity and affinity. *Chemistry and Biology*, **2**: 633–638.

Ellington, A.D. and Szostak, J.W. (1990). In vitro selection of RNA molecules that bind specific ligands. *Nature*, **346** (30): 818–822.

Entzian, C. and Schubert, T. (2016). Studying small molecule-aptamer interactions using MicroScale Thermophoresis (MST). *Methods*, **97**: 27–34.

Espiritu, C.A, Justo, C.A.C., Jauset Rubio, M., Svobodova, M., Bashammakh, A.S., Alyoubi, A.O., Rivera, W.L., Rollon, A.P. and O’Sullivan C.K. (2018). Aptamer selection against *Trichomonas vaginalis* adhesion protein for diagnostic application. *ACS Infectious Diseases*, **4**: 1306–1315.

Estruch, R., Ros, E., Salas-Salvadó, J., Covas, M., Corella, D., Arós, F., Gómez-Gracia, E., Ruiz-Gutiérrez, V., Fiol, M., Lapetra, J., Lamuela-Raventos, R.M., Serra-Majem, L., Pintó, X., Basora, J., Muñoz, M.A., Sorlí, J.V., Martínez, J.A. and Martínez-González, M.A. (2013). Primary prevention of cardiovascular disease with a Mediterranean diet. *The New England journal of medicine*, **368**(14): 1279–1290.

Fang, X., Sen, A., Vicens, M. and Tan. W. (2003). Synthetic DNA Aptamers to detect Proteins Molecular Variants in a High-Throughput Fluorescence Quenching Assay. *ChemBioChem*, **4**(9): 829–834.

Festa, A., D’Agostino, R Jr., Tracy, R.P. and Haffner, S.M. (2002). Insulin Resistance Atherosclerosis Study Elevated levels of acute-phase proteins and plasminogen activator inhibitor-1 predict the development of type 2 diabetes: the insulin resistance atherosclerosis study. *Diabetes*, **51**(4): 1131–1137.

Florinel-Gabriel, B. (2012). *Chemical Sensors and Biosensors: Fundamentals and Applications*. Chichester, UK: John Wiley & Sons. 576. ISBN 9781118354230

Gatto, B., Palumbo, M. and Sissi, C. (2009). Nucleic acid aptamers based on the G-quadruplex structure: therapeutic and diagnostic potential. *Current Medicinal Chemistry*, **16**: 1248–1265

Gold, L. and Tuerk, C. (1993). Methods for identifying nucleic acid ligands. US5270163

Gold, L.B.P., Uhlenbeck, O. and Yarus, M. (1995). Diversity of oligonucleotide functions. *Annual Review of Biochemistry*, **64**: 763–797.

Gopinath, S.C., Lakshmipriya, T., Chen, Y., Phang, W.M. and Hashim, U. (2016). Aptamer-based ‘point-of-care testing, *Biotechnology Advances*, **34**: 198–208.

Graham, T.E., Yang, Q., Bluher, M., Hammarstedt, A., Ciaraldi, T.P., Henry, R.R., Wason, C.J., Oberbach, A., Jansson, P.A., Smith, U. and Kahn, B.B. (2006). Retinol-binding protein 4 and insulin resistance in lean, obese, and diabetic subjects. *New England Journal of Medicine*, **354**: 2552–2563.

Groop, L. and Pociot, F. (2013). Genetics of diabetes - Are we missing the genes or the disease? *Molecular and Cell Endocrinology*, **25**(1): 726–739.

Guo, L.H. and Kim, D.H. (2012). LSPR biomolecular assay with high sensitivity induced by aptamer-antigen-antibody sandwich complex. *Biosensors and Bioelectronics*, **31**: 567–750.

Han, H.S., Kang, G., Kim J.S, Chooi, B. and Koo S.H. (2016). Regulation of glucose metabolism from a liver-centric perspective. *Experimental and Molecular Medicine*, **48**: e218; doi:10.1038/emm.2015.122

Hermann, T. and Patel, D.J. (2000). Adaptive Recognition by Nucleic Acid Aptamers. *Science*, **287**: 820–825.

Henry, N.L. and Hayes D.F. (2012). Cancer biomarkers. *Molecular Oncology*, **6**(2):140–146.

Hirtz, C., Chevalier, F., Sommerer, N., Raingeard, I., Bringer, J., Rossignol, M. de Périere D.D. (2006). Salivary protein profiling in type I diabetes using two-dimensional electrophoresis and mass spectrometry. *Clinical Proteomics*, **2**: 117–127.

Hoinka, J., Zotenko, E., Friedman A., Sauna, Z.E. and Przytycka T.M. (2012). Identification of sequence–structure RNA binding motifs for SELEX-derived aptamers. *Bioinformatics*, **28**(12): i215-23.

Hyle, E.P., Jani, I.V., Lehe, J., Su, A.E., Wood, R., Quevedo, J., Losina, E., Bassett, I.V., Pei, P.P., Paltie, D.A., Resch, S., Freedberg, K.A., Peter, T. and Walensky, R.P. (2014). The Clinical and Economic Impact of Point-of-Care CD4 Testing in Mozambique and Other Resource-Limited Settings: A Cost-Effectiveness Analysis. *PLoS Medicine*, **11**(9): 1–15.

Hu, J., Wang, S., Wang, L., Li, F., Pingguan-Murphy, B., Lu, T.J. and Xu, F. (2014). Advances in paper-based point-of-care diagnostics. *Biosensors and Bioelectronics*, **54**: 585–597.

Hung, P.H., Lu, Y.C., Chen, Y.W., Chou, H.C., Lyu, P.C., Lee, Y.R. and Chan, H.L. (2011). Proteomic identification of plasma signatures in type 2 diabetic nephropathy. *Journal of Integrated Omics*, **1**(1): 151–156.

Hurst, S.J., Lytton-Jean, A.K. and Mirkin, C.A. (2006). Maximizing DNA loading on a range of gold nanoparticle sizes. *Analytical Chemistry*, **78**: 8313–8318.

Insel, R.A., Dunne, J.L., Atkinson, M.A., Chiang, J.L., Dabelea, D., Gottlieb, P.A., Greenbaum C.J., Herold, K.C., Krischer, J.P., Lernmark, A., Ratner, R.E., Rewers, M.J., Schatz, D.A., Skyler, J.S., Sosenko, J.M. and Ziegler, A.G. (2015). Staging Presymptomatic Type 1 Diabetes: A Scientific Statement of JDRF, the Endocrine Society and the American Diabetes Association. *Diabetes Care*, **38**: 1964–1974.

International Diabetes Federation (IDF). (2018) Diabetes atlas - Home. Available: <http://www.diabetesatlas.org/>. (Retrieved April 2018)

International Diabetes Federation (IDF). (2017) Diabetes Atlas. 8th edition, 2017. Available: <http://www.diabetesatlas.org/resources/>. (Retrieved 03 May 2018).

Invitrogen (2010) Molecular Probes Handbook: A Guide to Fluorescent Probes and Labeling Technologies. Invitrogen, Waltham, MA, USA.

James, W. (2000). Aptamers. In: Meyers, R.A. (Ed.), Encyclopedia of Analytical Chemistry. John Wiley & Sons Ltd., Chichester, 4848–4871.

Järvelä, I.Y., Juutinen, J., Koskela, P., Hartikainen, A.L., Kulmala, P., Knip, M. and Tapanainen, J.S. (2006). Gestational diabetes identifies women at risk for permanent type 1 and type 2 diabetes in fertile age: Predictive role of autoantibodies. *Diabetes Care*, **29** (3): 607–612.

Jauset-Rubio, M., El-Shahawi M.S., Bashammakh A.S., Alyoubi A.O. and O'Sullivan C.K. (2017). Advances in aptamers-based lateral flow assays. *Trends in Analytical Chemistry*, **97**: 385–398.

Jauset-Rubio, M., Svobodova, M., Mairal, T., McNeil, C., Keegan, N., El-Shahawi, M.S., Bashammakh, A.S., Alyoubi, A.O. and O'Sullivan C.K. (2016). Aptamer lateral flow assays

for ultrasensitive detection of beta-conglutin combining recombinase polymerase amplification and tailed primers, *Analytical Chemistry*, **88**(21): 10701–10709.

Jauset-Rubio, M., Svobodová, M., Mairal, T., Schubert, T., Künne, S., Mayer, G. and O'Sullivan, C.K. (2016). β -Conglutin dual aptamers binding distinct aptotopes. *Analytical and Bioanalytical Chemistry*, **408**(3): 875–884.

Jenison, R.D., Gill, S.C., Pardi, A. and Polisky, B. (1994). High-resolution molecular discrimination by RNA. *Science*, **263**: 1425–1429.

Joubert, J., Norman, R, Bradshaw, D., Goedecke, J.H., Steyn, N.P. and Puoane, T. (2007). Estimating the burden of disease attributable to excess body weight in South Africa in 2000. *South African Medical Journal*, **97**: 683–90.

Kaku, K. (2010). Pathophysiology of Type 2 Diabetes and its treatment policy. *Japan Medical Association Journal*, **53**(1): 41–46.

Kamnev, A. A. (2013). Infrared Spectroscopy in Studying Biofunctionalised Gold Nanoparticles. *Nanomaterials Imaging Techniques, Surface Studies, and Applications*, **146**: 35–50.

Kapustin, J.F (2008). Postpartum management for gestational diabetes mellitus: Policy and practice implications. *Journal of the American Academy of Nurse Practitioners*, **20**: 547–554

Keefe, A.D., Pai, S. and Ellington, A. (2010). Aptamers as therapeutics. *Nature Reviews Drug Discovery*, **9**: 537–550.

Kengne, A.P., Echouffo-Tcheugui, J.B., Sobngwi, E., and Mbanya J.C. (2013). New insights on diabetes mellitus and obesity in Africa-part 1: prevalence, pathogenesis and comorbidities. *Heart*, **99**(14): 979–983.

Kim, S.E., Ahn, K.Y., Park, J.S., Kim, K.R., Lee, K.E., Han, S.S. and Lee, J. (2011). Fluorescent Ferritin Nanoparticles and Application to the Aptamer Sensor. *Analytical Chemistry*, **83**(15):5834–5843.

Koczula, K.M. and Gallotta, A. (2016). Lateral flow assays. *Essays in Biochemistry*, **60**: 111–120.

Kolberg J. A., Jorgensen T., Gerwien R. W., Hamren, S., McKenna, M.P., Moler, E., Rowe, M.W., Urdea, M.S., Xu, X.M., Hansen, T., Pedersen, O. and Borch-Johnsen, K. (2009). Development of a type 2 diabetes risk model from a panel of serum biomarkers from the Inter99 cohort. *Diabetes Care*, **32**(7): 1207–1212.

Kumar, B., Smita, K., Cumba L., Debut, A. and Pathak, R.N. (2014). Sonochemical Synthesis of Silver Nanoparticles Using Starch: A Comparison. *Bioinorganic Chemistry and Applications*, 2014:784268.

Kumar, P.J. and Clark, M. (2002). Textbook of Clinical Medicine. Pub: Saunders, London, UK. 1099–1121.

Kaur, H. and Yung L-Y.L. (2012). Probing High Affinity Sequences of DNA Aptamer against VEGF165. *PLoS One*, **7**(2): e31196.

Lauridsen, L.H., Shamaileh, H.A., Edwards, S.L., Taran, E. and Veedu, R.N. (2012). Rapid One-Step Selection Method for Generating Nucleic Acid Aptamers: Development of a DNA Aptamer against a-Bungarotoxin. *PLoS One*, **7**(7): e41702.

Lee, Y.J., Han, S.R., Maeng, J.S., Cho, Y.J. and Lee, S.W. (2012). In vitro selection of Escherichia coli O157:H7-specific RNA aptamer. *Biochemical and Biophysical Research Communications*, **417**: 414–420.

Lee, S.J., Youn, B., Park, J.W., Niazi, J.H., Kim, S.K. and Gu, M.B. (2008). SsDNA APTAMER-BASED Surface Plasmon Resonance biosensor for the detection of Retinol Binding Protein 4 for the early detection if Type 2 Diabetes. *Analytical Chemistry*, **80**: 2867–2873.

Lenčová, E., Broukal, Z. and Spížek, J. (2010). Point-of-care salivary microbial tests for detection of cariogenic species-clinical relevance thereof-review, *Folia Microbiologica*, **55**(6): 559–568.

Li, L., Yang, G., Li, Q., Tang, Y., Yang, M., Yang, H. and Li, K. (2006). Changes and relations of circulating visfatin, apelin, and resistin levels in normal, impaired glucose tolerance, and type 2 diabetic subjects. *Experimental and Clinical Endocrinology and Diabetes*, **114**(10): 544–548.

Li, J., Jing, L., Song, Y., Zhang J., Chen, Q., Wang, B., Xia, X. and Han, Q. (2018). Rapid detection of Rongalite via a sandwich lateral flow strip assay using a pair of aptamers. *Nanoscale Research Letters*, **13**(1): 296.

Lin, H.I., Wu, C.C., Yang, C.H., Chang, K.W., Lee, G.B and Shiesh, S.C. (2015) Selection of aptamers specific for glycated haemoglobin and total haemoglobin using on-chip SELEX. *Lab Chip*, **15**(2): 486–494.

Liu, J., Cao, Z. and Lu, Y. (2009). Functional nucleic acid sensors. *Chemical Review*, **109**(5): 1948–1998.

Liu, G.D., Mao, X., Phillips, J.A., Xu, H., Tan, W.H. and Zeng, L.W. (2009). Aptamer-Nanoparticle Strip Biosensor for Sensitive Detection of Cancer Cells. *Analytical Chemistry*, **81**: 10013–10018.

Liu, J. and Lu, Y. (2006). Preparation of aptamer-linked gold nanoparticle purple aggregates for colorimetric sensing of analytes. *Nature Protocols*, **1**: 246–252.

Lowe, J., Taveira-da-Silva, R. and Hilario-Souz, E. (2017). Dissecting Copper Homeostasis in Diabetes Mellitus. *International Union of Biochemistry and Molecular Biology Life*, **69**(4): 255–262.

Lowe W.L. and Karban J. (2015). Genetics, genomics and metabolomics: new insights into maternal metabolism during pregnancy. *Diabetic Medicine*, **31**(3): 254–262.

Lowe, W.L (2005). Principles of Molecular Medicine, Humana Press, New Jersey, NJ, USA, 16th edition.

Luong, J.H., Male, K.B. and Glennon, J.D. (2008). Biosensor technology: technology push versus market pull. *Biotechnology Advances*, **26**(5): 492–500.

Malamud, D. (2011). Saliva as a Diagnostic Fluid. *Dental Clinics of North America*, **55**(1) 159–178.

Malathi, N., Mythili, S. and Vasanthi, H.R. (2014). Salivary diagnostics: a brief review. *ISRN dentistry*, 158786.

Mallikaratchy, P., Tang, Z., Kwame, S., Meng, L., Shangguan, D. and Tan, W. (2007) Aptamer directly evolved from live cells recognizes membrane bound immunoglobulin heavy mu chain in Burkitt's lymphoma cells. *Molecular and Cell Proteomics*, **6**(12): 2230–2238.

Mao, X., Phillips, J.A., Xua, H., Tanb, W., Zengc, L. and Liua, G. (2009). Aptamer-Nanoparticle Strip Biosensor for Rapid and Sensitive Detection of Cancer Cell. *Analytical Chemistry*, **81**(24): 1001–1008.

Mason, J.M., Hancock, H.C., Close, H., Murphy, J.J., Fuat, A., de Belder, M., Singh, R., Teggert, A., Wood, E., Brennan, G., Hussain, N., Kumar, N., Manshani, N., Hodges, D., Wilson, D. and Hungin, A.P.S. (2013). Utility of Biomarkers in the Differential Diagnosis of Heart Failure in Older People: Findings from the Heart Failure in Care Homes (HFinCH) Diagnostic Accuracy Study. *PLoS ONE*, **8**(1), e53560.

McDermott, J.E., Wang, J., Mitchell, H., Webb-Robertson, B., Hafen, R., Ramey, J., and Rodland, K.D. (2013). Challenges in Biomarker Discovery: Combining Expert Insights with Statistical Analysis of Complex Omics Data. *Expert Opinion on Medical Diagnostics*, **7**(1): 37–51.

Mendonsa, S.D and Bowser, M.T. (2004). In vitro selection of high-affinity DNA ligands for human IgE using capillary electrophoresis. *Analytical Chemistry*, **76**(18): 5387–5392.

Melmed, S., Kenneth, P., Larsen, P.R. and Henry, K. (eds.). Williams textbook of endocrinology (12th ed.). *Philadelphia: Elsevier/Saunders*, 1371–1435. ISBN 978-1-4377-0324-5.

Miller, K., Kim, A., Kilimnik, G., Jo, J., Moka, U., Periwal, V. and Hara, M. (2009). Islet formation during the neonatal development in mice. *PLoS One*, **4**(11): e7739.

Millipore (2009) Rapid Lateral Flow Test Strips: Consideration for Product Development. <http://www.millipore.com/techpublications/tech1/tb500en500>.

Molesworth, A.M., Ndhlovu, R., Banda, E., Saul, J., Ngwira, B., Glynn, J.R., Crampin, A.C. and French, N. (2010). High accuracy of home-based community rapid HIV testing in rural Malawi. *Journal of Acquired Immune Deficiency Syndromes*, **55**(5): 625–30.

Mondal, B., Ramlal, S., Lavu, P.S., Bhavanashri, N. and Kingston, J. (2018). Highly Sensitive Colorimetric Biosensor for Staphylococcal Enterotoxin B by a Label-Free Aptamer and Gold Nanoparticles. *Frontiers in Microbiology*, **9**: 179. doi: 10.3389/fmicb.2018.00179

Morales-Narvaez, E., Naghdi, T., Zor, E. and Merkoci, A. (2015). Photoluminescent lateral-flow immunoassay revealed by graphene oxide: highly sensitive paper-based pathogen detection. *Analytical Chemistry*, **87**: 8573–8577.

Mosing, R.K., Mendonsa, S.D. and Bowser, M.T. (2005). Capillary electrophoresis-SELEX selection of aptamers with affinity for HIV-1 reverse transcriptase. *Analytical Chemistry*, **77**: 6107–6112.

Nadal, P., Pinto, A., Svobodova, M., Canela, N. and O’Sullivan, C.K. (2012). DNA aptamer against Lup an 1 food allergen. *PLoS ONE*, **7**(4): e35253.

Nakanishi, T., Koyama, R., Ikeda, T. and Shimizu A. (2002). Catalogue of soluble proteins in the human vitreous humor: comparison between diabetic retinopathy and macular hole. *Journal of Chromatography B: Analytical Technologies in the Biomedical and Life Sciences*, **776**(1): 89–100.

Nanocomposix. (2012). Zeta Potential Analysis of Nanoparticles. *NanoComposix*, **11**: 1-6.

Nara, S., Tripathi, V., Singh, H. and Shrivastav, T.G. (2010). Colloidal gold probe based rapid immunochromatographic strip assay for cortisol. *Analytica Chimica Acta*, **682**: 66–71.

Nathan, D.M., Cleary, P.A., Backlund, J.Y., Genuth, S.M., Lachin, J.M., Orchard, T.J., Raskin, P., Zinman, B. and Diabetes Control and Complications Trial/Epidemiology of Diabetes Interventions and Complications (DCCT/EDIC) Study Research Group (2005). Intensive diabetes treatment and cardiovascular disease in patients with type 1 diabetes. *The New England Journal of Medicine*, **353**(25): 2643–53.

Newcomer, M.E. and Ong, D.E. (2000). Plasma retinol binding protein: structure and function of the prototypic lipocalin. *Biochimica et Biophysica Acta*, **1482**: 57–64.

Newmand, J.D. and Setford, S.J. (2006). Enzymatic biosensors. *Molecular Biotechnology*, **32**: 249–268.

Ng, M., Fleming, T., Robinson, M., Thomson, B., Graetz, N., and Margono, C. (2014). Global, regional, and national prevalence of overweight and obesity in children and adults during 1980-2013: a systematic analysis for the Global Burden of Disease Study 2013. *Lancet*, **384** (9945):766–781.

Ngo V.K.T., Nguyen H.P.U., Huynh T.P., Tran N.N.P., Lam Q.V. and Huynh T.D. (2015). Preparation of gold nanoparticles by microwave heating and application of spectroscopy to study conjugate of gold nanoparticles with antibody E. coli O157:H7. *Advances in Natural Sciences: Nanoscience and Nanotechnology*, **6** (3): e35016.

Ngom, B., Guo, Y., Wang, X. and Bi, D. (2010). Development and application of lateral flow test strip technology for detection of infectious agents and chemical contaminants: a review. *Analytical and Bioanalytical Chemistry*, **397**: 1113–1135.

Nitsche, A., Kurth, A., Dunkhorst, A., Pänk, O., Sielaff, H., Junge, W., Muth, D., Scheller, F., Stöcklein, W., Dahmen, C., Pauli, G. and Kage A. (2007). One-step selection of Vaccinia virus-binding DNA aptamers by MonoLEX. *BMC Biotechnology*, **7**(48): 18–23.

Nomiyama, T. and Yanase, T. (2015). Secondary diabetes. *Nihon Rinsho*, **73**(12):2008–2012.

Onat, A., Hergenç, G., Bulur, S., Ugur, M., Kuçukdurmaz Z and Can G (2010). The paradox of high apo- lipoprotein A-I levels independently predicting incident type-2 diabetes among Turks. *International Journal of Cardiology*, **142**: 72–79.

Ooi, C.P. and Loke, S.C. (2012). Colesevelam for type 2 diabetes mellitus. *The Cochrane Database of Systematic Reviews*, **12**: CD009361. Ottermann, B. (2012). Prevalence of diabetes in South Africa. Available: <http://www.health24.com/Medical/Diabetes/About-diabetes/Diabetes-tsunamihits-South-Africa20130210>. (Retrieved May 2018).

Ou, L.J., Jin, P.Y., Chu, X., Jiang, J.H., Yu, R.Q. (2010). Sensitive and Visual Detection of Sequence-Specific DNA-Binding Protein via a Gold Nanoparticle-Based Colorimetric Biosensor. *Analytical Chemistry*, **82**: 6015–6024.

Panchbhai, A.S. (2012). Correlation of salivary glucose level with blood glucose level in diabetes mellitus. *Journal of Oral Maxillofacial Research*, **3**(3):1–6.

Panda, A., Venkatapathy, R. and Oza, N. (2012). Glucose estimation in the salivary secretion of diabetes mellitus patients: diabetes, metabolic syndrome and obesity. *Targets and Therapy*, **5**: 149–54.

Peer, N., Kengne, A.P., Motala, A.A., Mbanya, J.C. (2014). Diabetes in the Africa region: an update. *Diabetes Research and Clinical Practice*, **103**: 197–205.

Pendergrast, P.S., Marsh, H.N., Grate, D., Healy, J.M., Stanton, M. (2005). Nucleic acid aptamers for target validation and therapeutic applications. *Journal of biomolecular techniques*, **16**(3): 224–234.

Philip, D. (2008). Synthesis and spectroscopic characterization of gold nanoparticles. *Spectrochimica Acta. Part A, Molecular and Biomolecular Spectroscopy*, **71**(1): 80–85.

Piganeau, N. and Schroeder, R. (2003). Aptamer structures: a preview into regulatory pathways? *Chemical Biology*, **10**(2): 103–104.

Pociot, F. and Lernmark, A. (2016). Genetic risk factors for type 1 diabetes. *The Lancet*, **387**(10035): 2331–2339.

Porta, M., Toppila, I., Sandholm, N., Hosseini, S.M., Forsblom, C., Hietala, K., Borio, L., Harjutsalo, V., Klein, B.E., Klein, R., Paterson A.D. and Per-Henrik Groop P-H. (2016). Variation in SLC19A3 and Protection from Microvascular Damage in Type 1 Diabetes. *Diabetes*, **65**(4): 1022–1030.

Peer, D., Karp, J.M., Hong, S., FarokHzad, O.C., Margalit, R. and Langer, R. (2007). Nanocarriers as an emerging platform for cancer therapy. *Nature Nanotechnology*, **2**: 751 – 760.

Pultar, J., Sauer, U., Domnanich, P. and Preininger, C. (2009). Aptamer-antibody on-chip sandwich immunoassay for detection of CRP in spiked serum. *Biosensors and Bioelectronics*, **24**: 1457–1461.

Qadami, F., Molaeirad, A., Alijanianzadeh, M., Azizi, A. and Kamali, N. (2018). Localized Surface Plasmon Resonance (LSPR)-Based Nanobiosensor for Methamphetamine Measurements. *Plasmonics*, **13**: 2091–2098.

Quesada-González, D. and Merkoçi, A.M. (2018). Nanomaterial-based devices for point-of-care diagnostic applications. *Chemical Society Reviews*, **47**(13): 4697–4709.

Rao, P.V., Reddy, A.P., Lu, X., Dasari, S., Krishnaprasad, A., Biggs, E., Roberts, C.T. and Nagalla, S.R. (2009). Proteomic identification of salivary biomarkers of type 2 diabetes. *Journal of Proteome Research*, **8**(1): 239–245.

Rao, C.N.R. and Biswas, K. (2009). Characterization of nanomaterials by physical methods. *Annual Review of Analytical Chemistry*, **2**: 435–462.

Raston, N.H.A., Nguyen, V.T. and Gu, M.B. (2017). A new lateral flow strip assay (LFSA) using a pair of aptamers for the detection of Vaspin. *Biosensors and Bioelectronics*, **93**: 21–25.

Raston, N.H.A. and Gu, M.B. (2015). Highly amplified detection of visceral adipose tissue derived serpin (vaspin) using a cognate aptamer duo. *Biosensors and Bioelectronics*, **70**: 261–267.

Rey, E., O'Dell, D, Mehta, S. and Erickson D. (2017). Mitigating the hook effect in lateral flow sandwich immunoassays using real-time reaction kinetics. *Analytical Chemistry*, **89**(9): 5097–5100.

Riaz, S. (2009). Diabetes mellitus. *Scientific Research and Essays*, **4**(5): 367–373.

Rodriguez, Z.J. and O'Kennedy, R. (2017). New approaches for the development of diagnostic systems. *Medical Sciences*, **38**: 18–23.

Sajid, M., Kawde A. and Daud, M. (2015). Designs, formats and applications of lateral flow assay: A literature review. *Journal of Saudi Chemical Society*, **19**(6): 689–705.

Sajid, V.S., Choe, H.C. and Young, K.W.K. (2010). Nanotechnology in biomedical applications - a review. *International Journal of Nano Biomaterials*, **3**: 119–139.

Sasongko, M.B., Wong, T.Y., Nguyen, T.T., Kawasaki, R., Jenkins, A., Shaw, J. and Wang, J.J. (2011) Serum apolipoprotein AI and B are stronger biomarkers of diabetic retinopathy than traditional lipids. *Diabetes Care*, **34**(2): 474–479.

Schütze T., Wilhelm, B., Greiner, N., Braun, H., Peter, F., Mörl, M., Erdmann, V.A., Lehrach, H., Konthur, Z., Menger, M., Arndt, P.F. and Glökler, J. (2011). Probing the SELEX Process with Next-Generation Sequencing. *PLoS One*, **6**(12): e29604.

Setlem, K., Mondal, B., Ramlal, S. and Kingston, J. (2016). Immuno affinity selex for simple, rapid, and cost-effective aptamer enrichment and identification against aflatoxin B1. *Frontiers in Microbiology*, **7**: e1909.

Sharma, T.K., Bruno, J.G. and Dhiman, A. (2017). ABCs of DNA aptamer and related assay development. *Biotechnology Advances*, **35** (2): 275–301.

Sharma, T. K., Bruno, J. G., and Cho, W. C. (2016). The point behind translation of aptamers for Point of Care Diagnostics. *Aptamers and Synthetic Antibodies*, **3**(1): 36–42.

Sharma S, Julia Zapatero-Rodríguez, Estrela P and O’Kennedy R (2015). Point-of-Care Diagnostics in Low Resource Settings: Present Status and Future Role of Microfluidics. *Biosensors-Basel*, **5**(3): 577–601.

Sharma, T.K. and Shukla, R. (2014). Nucleic acid aptamers as an emerging diagnostic tool for animal pathogens. *Advances in Animal and Veterinary Sciences*, **2**: 50–55.

Shen, G., Zhang, S. and Hu, X. (2013). Signal enhancement in a lateral flow immunoassay based on dual gold nanoparticle conjugates, *Clinical Biochemistry*. **46**(16-17): 1734–1738.

Shim, W.B., Kim, M.J., Mun, H. and Kim, M.G. (2014). An aptamer-based dipstick assay for the rapid and simple detection of aflatoxin B1. *Biosensors and Bioelectronics*, **62**: 288–294.

Shukla, S., Leem, H., Lee, J.S. and Kim, M. (2014). Immunochromatographic strip assay for the rapid and sensitive detection of Salmonella Typhimurium in artificially contaminated tomato samples. *Canadian Journal Microbiology*, **60**: 399–406.

Shoback, D. (2011). Chapter 17. Greenspan's basic and clinical endocrinology (9th ed.). New York: McGraw-Hill Medica.

Schüling, T., Eilers, A., Scheper, T. and Walter, J. (2018). Aptamer-based lateral flow assays. *AIMS Bioengineering*, **5**(2): 78–102.

Sibuyi, N.R.S., Thovhogi, N., Gabuza, K.B., Meyer, M.D., Drah, M., Onani, M.O., Skepu, A., Madiehe, A.M. and Meyer M. (2017). Peptide-functionalized nanoparticles for the selective induction of apoptosis in target cells. *Nanomedicine*, **12**: 1631–1645.

Song, Y., Huang, Y.Y., Liu, X., Zhang, X., Ferrari, M. and Qin, L. (2014). Point-of-care technologies for molecular diagnostics using a drop of blood. *Trends in Biotechnology*, **32**: 132–139.

Song, K.M., Lee, S., Ban, C. (2012). Aptamers and their biological applications. *Sensors*, **12**: 612–631.

Stenström, G., Gottsäter, A., Bakhtadze, E., Berger, B., Sundkvist, G. (2005). Latent autoimmune diabetes in adults: definition, prevalence, beta-cell function, and treatment. *Diabetes*, **54**(2): 68–72.

Stofkova, A. (2010). Resistin and visfatin: regulators of insulin sensitivity, inflammation and immunity. *Endocrine Regulations*, **44**(1): 25–36.

Stoltenburg, R., Schubert, T. and Strhlitz, B. (2015). In vitro selection and interaction studies of a DNA aptamer targeting Protein A. *PLoS One*, **10**(7): e1034403.

Stoltenburg, R., Reinemann, C. and Strehlitz, B. (2005). FluMag-SELEX as an advantageous method for DNA aptamer selection. *Analytical and Bioanalytical Chemistry*, **383**(1): 83–91

Strimbu, K. and Tavel J.A. (2010). What are biomarkers? *Current opinion in HIV and AIDS*, **5**(6): 463–466.

Sun, H. and Zu, Y. (2015). A Highlight of Recent Advances in Aptamer Technology and Its Application. *Molecules*, **20**: 11959-11980.

Sun, J.K., Keenan, H.A., Cavallerano J.D., Asztalos, B.F., Schaefer, E.J., Sell, D.R., Strauch, C.M., Monnier, V.M., Doria, A., Paul Aiello, L. and King G.L. (2011). Protection from Retinopathy and Other Complications in Patients with Type 1 Diabetes of Extreme Duration. *Diabetes Care*, **34**(4): 968–974.

Sun, L., Qi, Q., Zong, G., Ye, X., Li, H., Liu, X., Zheng, H., Hu, F.B, Liu, Y. and Lin, X. (2014). Elevated plasma retinol-binding protein 4 is associated with increased risk of type 2

diabetes in middle-aged and elderly Chinese adults. *The Journal of Nutrition*, **144**(5): 722–728.

Sundsten, T. and Ortsäter, H. (2009). Proteomics in diabetes research. *Molecular and Cellular Endocrinology*, **297**: 93–103.

Srinivasan, B. and Tung, S. (2015). Development and Applications of Portable Biosensors. *Journal of Laboratory Automation*, **20**(4): 365–389.

Svobodová, M., Pianto, A., Nadal, P. and O'Sullivan, C.K. (2012). Comparison of different methods for generation of single-stranded DNA for SELEX processes. *Analytical and Bioanalytical Chemistry*, **404**(3): 835–842

Sypabekova, M., Bekmurzayeva, A., Wang, R., Li, Y., Nogue, C. and Kanayeva, D. (2017). Selection, characterization, and application of DNA aptamers for detection of Mycobacterium tuberculosis secreted protein MPT64. *Tuberculosis*, **104**: 70–78.

Tang, Z.W., Shangguan, D., Wang, K.M., Shi, H., Sefah, K., Mallikratchy, P., Chen, H.W., Li, Y. and Tan, W.H. (2007). Selection of aptamers for molecular recognition and characterization of cancer cells. *Analytical Chemistry*, **79**: 4900–4907.

Takebayashi K., Suetsugu M., Wakabayashi S., Aso, Y. and Inukai, T. (2007). Retinol binding protein-4 levels and clinical features of type 2 diabetes patients. *The Journal of Clinical Endocrinology and Metabolism*, **92**(7): 2712–2719.

Tejaswi, M., Rao, M.C., Datta Prasad, P.V., Giridhar, G., Pisipti, V.G.K.M. and Manepalli, R.K.N.R. (2006). Synthesis and characterization of citrate capped gold nanoparticles and their effect on liquid crystals: optical studies. *Rasayan journal of chemistry*, **9**(4): 697–705.

Thebani, A., Afonso, C., Marret, S. and Bekri, S. (2016). Omics-Based Strategies in Precision Medicine: Toward a Paradigm Shift in Inborn Errors of Metabolism Investigations. *International Journal of Molecular Sciences*, **17**(9): e1555.

Thobhani, S., Attree, S., Boyd, R., Kumarswami, N., Noble, J., Szymanski, M. and Porter, R.A. (2010). Bioconjugation and characterisation of gold colloid-labelled proteins. *Journal of Immunological Methods*, **356**: 60–69.

Tolle, F., Wilke, J., Wengel, J. and Mayer, G. (2014). By-Product Formation in Repetitive PCR Amplification of DNA Libraries during SELEX. *PLoS One*, **9**(12): e114693.

Uludag, Y., Narter, F., Sa lam, E., Kktrk, G., Gk, M.Y., Akgn, M., Barut, S. and Budak S. (2016). An integrated lab-on-a-chip-based electrochemical biosensor for rapid and sensitive detection of cancer biomarkers. *Analytical and Bioanalytical Chemistry*, **408**: 7775–7783.

Umeno, A., Yoshino, K., Hashimoto, Y., Schichiri, M., Kataota, M. and Yoshida, Y. (2015). Multi-Biomarkers for Early Detection of Type 2 Diabetes, Including 10- and 12-(Z,E) Hydroxyoctadecadienoic Acids, Insulin, Leptin, and Adiponectin. *PLoS One*, **10**(7): e0130971.

Unnikrishnan, R., Pradeepa, R., Joshi, S.R. and Mohan, V. (2017). Type 2 Diabetes: Demystifying the Global Epidemic. *Diabetes*, **66**: 1432–1442

Vaishya, S., Sarwade, R.D. and Seshadri, V. (2018). MicroRNA, proteins and metabolites as novel biomarkers for prediabetes, diabetes and related complications. *Frontiers in Endocrinology*, **9**: e80.

Verma, H.N., Sighn, P. and Chavan, R.M. (2014). Gold nanoparticles: synthesis and characterization. *Veterinary World*, **7**(2): 72–77.

Viglasky, V. and Hianik, T. (2013). Potential use of G-quadruplex-forming aptamers. *Physiology and Biophysics*, **32**: 149–172.

Vorster, H.H., Venter, C.S., Wissing, M.P. And Margetts, B.M. (2005). The nutrition and health transition in the North West Province of South Africa: a review of the THUSA (Transition and Health during Urbanisation of South Africans) study. *Public Health Nutrition*, **8**: 480–90.

Wang, J.P., Gong, Q., Maheshwar, N., Eisenstein, M., Arcila, M.L., Kosik, K.S. and Soh, H.T. (2014). Particle display: a quantitative screening method for generating high-affinity aptamers. *Angewandte Chemie International Edition*, **53**(19): 4796–4801.

Wang, Y., Luo, Y., Bing, T., Chen, Z., Lu, M., Zhang, N., Shanguan, D. and Gao, X. (2014). DNA Aptamer Evolved by Cell-SELEX for Recognition of Prostate Cancer. *PLoS One*, **9**(6): e100243.

Wang, C.F., Zhang, L.F. and Shen, X.M. (2013). Development of a nucleic acid lateral flow strip for detection of hepatitis C virus (HCV) core antigen. *Nucleosides Nucleotides Nucleic Acids*, **32**(2): 59–68.

Wang, L., Chen, W., Ma, W., Liu, L., Ma, W., Zhao, Y., Zhu, Y., Xu, L., Kuang, H. and Xu, C. (2011). Fluorescent strip sensor for rapid determination of toxins. *Chemical Communications*, **47**(5): 1574–1576

Wilcox, G. (2005). Insulin and insulin resistance. *The Clinical biochemist. Reviews / Australian Association of Clinical Biochemists*, **26**(2): 19–39.

Willett, W.C. and Leibel, R.L. (2002). Dietary Fat Is Not a Major Determinant of Body Fat. *American Journal of Medicine*, **113**(9B): 47–59.

World Health Organization (WHO). (2016) Global report on Diabetes. Available: <http://www.who.int/mediacentre/factsheets/fs312/en/>. (Retrieved: May 2018)

Wright, T.A. (2011). Salivary diagnostic testing: a "game changer" for patient evaluation. *Compendium of Continuing Education in Dentistry*, **32**(4): 28–29.

Wu, W., Zhao, S., Mao, Y., Fang, Z., Lu, X. and Zeng, L. (2015). A sensitive lateral flow biosensor for Escherichia coli O157:H7 detection based on aptamer mediated strand displacement amplification, *Analytica Chimica Acta*, **861**: 62–68.

Wu, Y., Ding, Y., Tanaka, Y. and Zhang, W. (2014). Risk Factors Contributing to Type 2 Diabetes and Recent Advances in the Treatment and Prevention. *International Journal of Medical Sciences*, **11**(11): 1185–1200.

Wu, H., Yu, Z., Qi, Q., Li, H., Sun, Q. and Lin, X. (2011). Joint analysis of multiple biomarkers for identifying type 2 diabetes in middle-aged and older Chinese: a cross-sectional study. *BMJ Open*, **1**(1): p. e000191.

Xiao, N., Long, Q., Tang, X. and Tang, S. (2014). A community-based approach to non-communicable chronic disease management within a context of advancing universal health coverage in China: progress and challenges. *BioMed Central*, **14**: 2–6.

Xu, Y., Tan, S., Liang, Q. and Ding M. (2007). One-Step Facile Synthesis of Aptamer-Modified Graphene Oxide for Highly Specific Enrichment of Human A-Thrombin in Plasma. *Sensors*, **17**: e1986.

Xu, H., Mao, X., Zeng, Q.X., Wang, S.F., Kawde, A.N. and Liu, G. D. (2009). Aptamer-functionalized gold nanoparticles as probes in a dry-reagent strip biosensor for protein analysis. *Analytical Chemistry*, **81**: 669–676.

Xu, J.W., Morita, I., Ikeda, K., Miki, T. and Yamori, Y. (2007). C-reactive protein suppresses insulin signalling in endothelial cells: role of spleen tyrosine kinase. *Molecular Endocrinology*, **21**: 564–573.

Xu, H., Mao, X., Zeng, Q., Wang, S., Kawde, A.N. and Liu, G. (2006). Aptamer-functionalized gold nanoparticles as probes in a dry-reagent strip biosensor for protein analysis. *Analytical Chemistry*, **81**: 669–675.

Yang, Q., Graham, T.E., Mody, N., Preitner, F., Peroni, O.D., Zabolotny, J.M., Kotani, K., Quadro, L. and Kahn, B.B. (2005). Serum retinol binding protein 4 contributes to insulin resistance in obesity and type 2 diabetes. *Nature*, **436**: 356–362.

Yu, L., Ng, S.R., Xu, Y., Dong, H., Wang, Y.J. and Li, C.M. (2013). Advances of lab-on-a-chip in isolation, detection and post-processing of circulating tumour cells. *Lab on a Chip*, **13**: 3163–3182.

Yudkin, J.S., Juhan-Vague, I., Hawe, E., Humphries, S.E., di Minno, G., Margaglione, M., Tremoli, E., Kooistra, T., Morange, P.E., Lundman, P., Mohamed-Ali, V. and Hamsten, A. (2004). Low-grade inflammation may play a role in the etiology of the metabolic syndrome in patients with coronary heart disease: the HIFMECH study. *Metabolism*, **53**: 852–857.

Zhang, X., Servo, M.R. and Liu, J. (2012). Surface science of DNA adsorption onto citrate-capped gold nanoparticles. *Langmuir*, **28**: 3896–3902.

Zhang, J., Wang, X.L. and Yang, X.R. (2012). Colorimetric determination of hypochlorite with unmodified gold nanoparticles through the oxidation of a stabilizer thiol compound. *Analyst*, **137**: 2806–2812.

Zhou, J., and Rossi, J. (2017). Aptamers as targeted therapeutics: current potential and challenges. *Nature Reviews Drug Discovery*, **16**: 181–202.

Zhou, W. L., Kong, W.J., Dou, X.W., Zhao, M., Ouyang, Z. and Yang, M.H. (2016). An aptamer based lateral flow strip for on-site rapid detection of ochratoxin A in *Astragalus membranaceus*. *Journal of chromatography. B, Analytical Technologies in the Biomedical and Life Sciences*, **1022**: 102–108.

Zhu, C., Zhao, Y., Yan, M., Huang, Y., Yan, J., Bai, W. and Chen, A. (2016). A sandwich dipstick assay for ATP detection based on split aptamer fragments. *Analytical and Bioanalytical Chemistry*, **408**: 4151–4158.

Zhu, G., Lübbecke, M., Walter, J.G., Stahl, F., Scheper, T. (2011). Characterization of Optimal Aptamer-Microarray Binding Chemistry and Spacer Design. *Chemical Engineering and Technology*, **34**: 2022–2028.

Zimbone, M., Baeri, P., Calcagno, L., Musumeci P., Contino, A. Barcellona, M.L and Bonaventura G. (2014). Dynamic light scattering on bioconjugated laser generated gold nanoparticles. *PLoS One*, **9**(3): e89048.

APPENDIX A: MULTIPLE SECONDARY STRUCTURES OF RBA-1

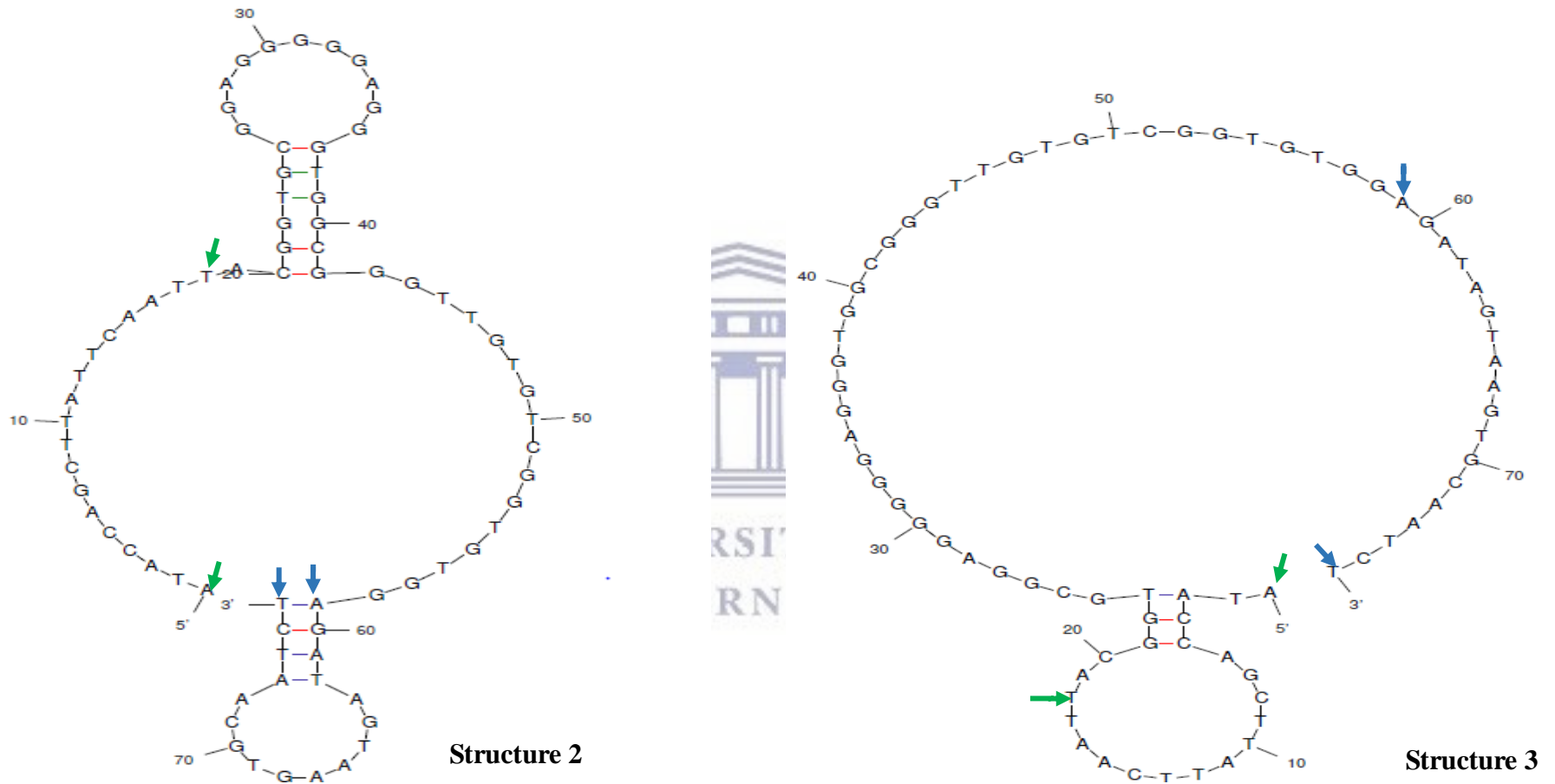


Figure A.1: Secondary structure prediction of RBA-1: (2) ($\Delta G = -0.18 \text{ kJ mol}^{-1}$) and (3) ($\Delta G = -0.06 \text{ kJ mol}^{-1}$) as predicted by the M-fold program. The ΔG represents the minimum free energy of each aptamer. The forward primer sequence (base 1-18) is shown by the green colour and the reverse primer (base 59-76) are shown by the blue colour.

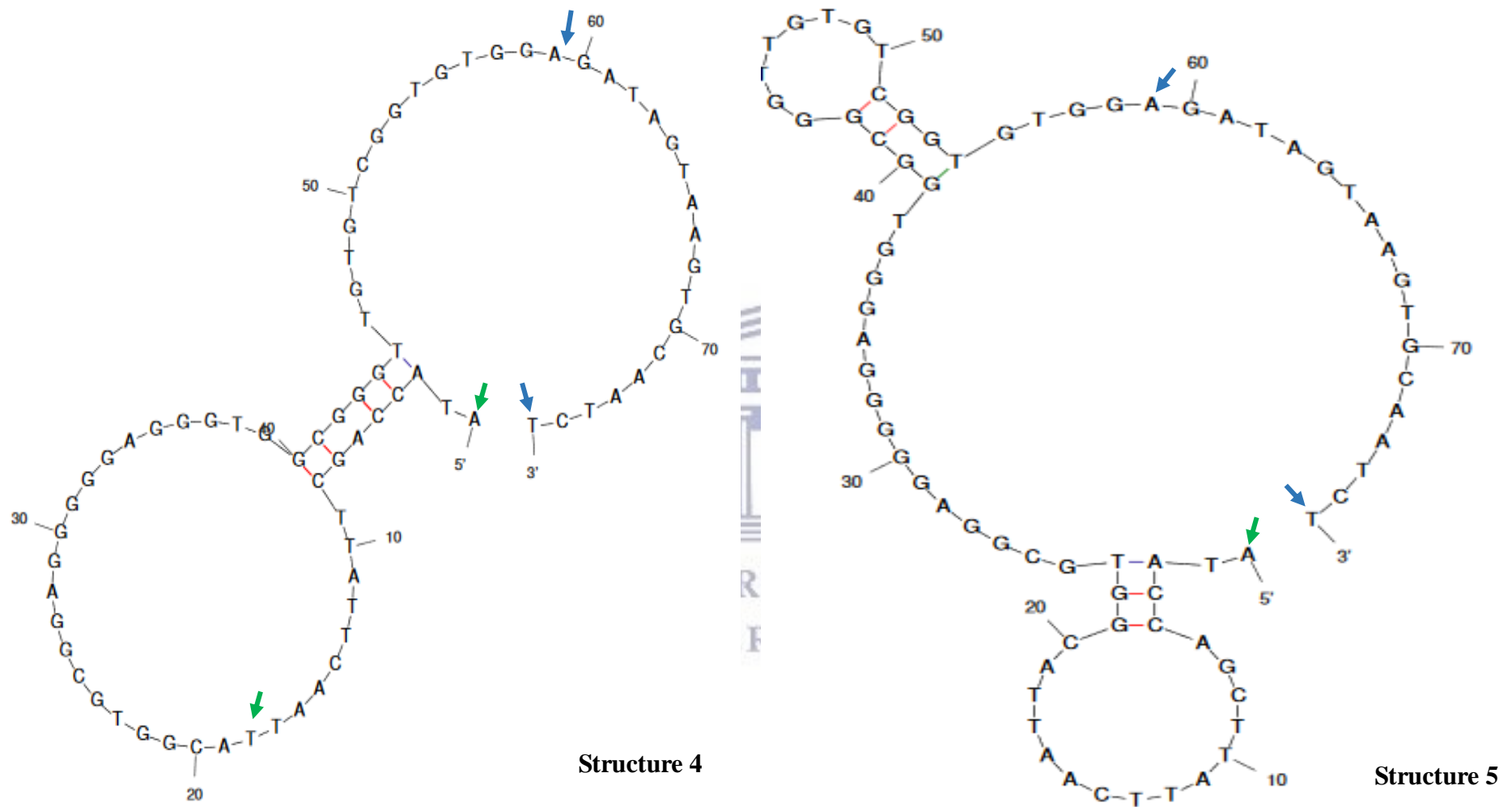
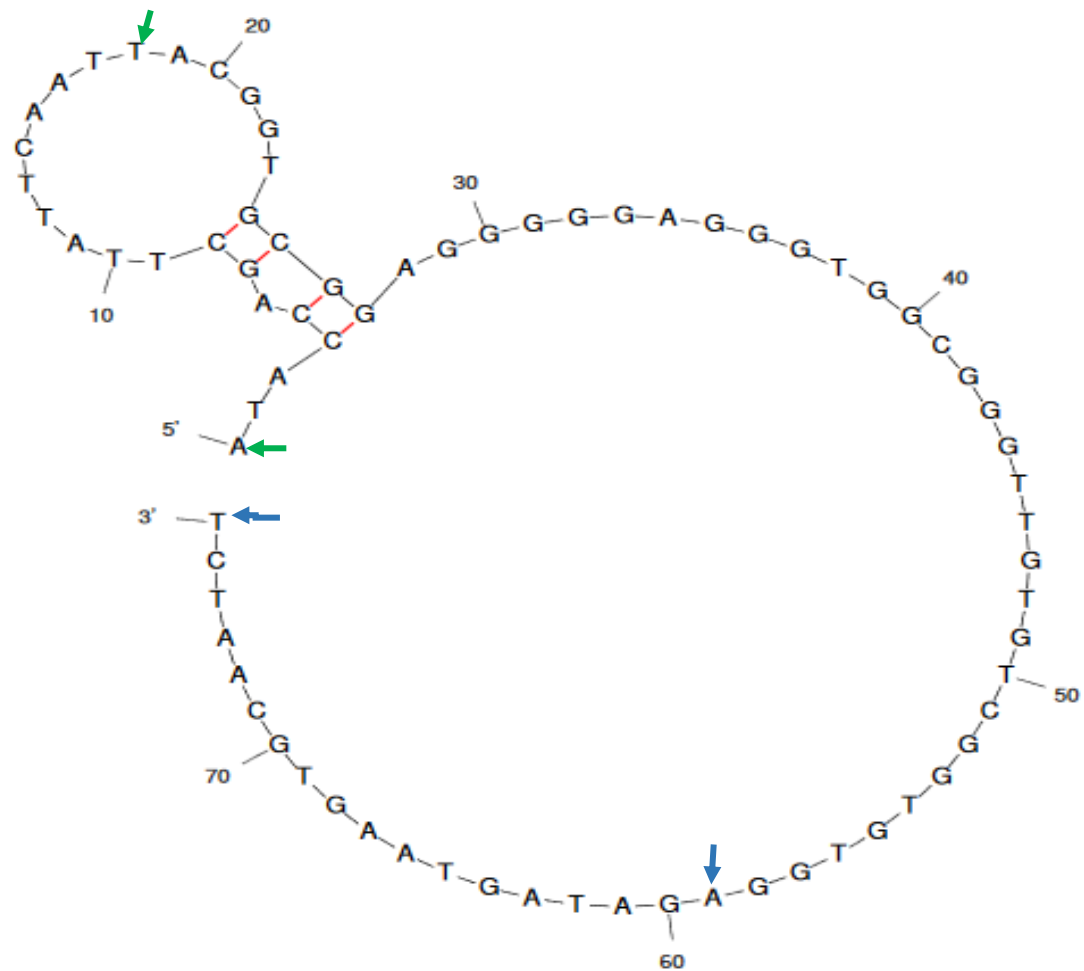


Figure A.2: Secondary structure prediction of RBA-1: (4) ($\Delta G = -0.04 \text{ kJ mol}^{-1}$) and (5) ($\Delta G = -0.43 \text{ kJ mol}^{-1}$) as predicted by the M-fold program. The ΔG represents the minimum free energy of each aptamer. The forward primer sequence (base 1-18) is shown by the green colour and the reverse primer (base 59-76) are shown by the blue colour.



Structure 6

Figure A.3:Secondary structure prediction of RBA-1: (5) ($\Delta G= -0.55 \text{ kJ mol}^{-1}$) as predicted by the M-fold program. The ΔG represents the minimum free energy of each aptamer. The forward primer sequence (base 1-18) is shown by the green colour and the reverse primer (base 59-76) are shown by the blue colour.